RI | 9525

REPORT OF INVESTIGATIONS/1994

Studies of Stope-Scale Seismicity in a Hard-Rock Mine

Part 1: Methods and Factors

By Robert L. Kranz, John P. Coughlin, and Selena Billington

UNITED STATES DEPARTMENT OF THE INTERIOR

BUREAU OF MINES

U.S. Department of the Interior
Mission Statement

As the Nation's principal conservation agency, the Department of the Interior has responsibility for most of our nationally–owned public lands and natural resources. This includes fostering sound use of our land and water resources; protecting our fish, wildlife, and biological diversity; preserving the environmental and cultural values of our national parks and historical places; and providing for the enjoyment of life through outdoor recreation. The Department assesses our energy and mineral resources and works to ensure that their development is in the best interests of all our people by encouraging stewardship and citizen participation in their care. The Department also has a major responsibility for American Indian reservation communities and for people who live in island territories under U.S. administration.

Report of Investigations 9525

Studies of Stope-Scale Seismicity in a Hard-Rock Mine

Part 1: Methods and Factors

By Robert L. Kranz, John P. Coughlin, and Selena Billington

UNITED STATES DEPARTMENT OF THE INTERIOR
Bruce Babbitt, Secretary

BUREAU OF MINES
Rhea L. Graham, Director

International Standard Serial Number
ISSN 1066-5552

CONTENTS

ILLUSTRATIONS

TABLE

UNIT OF MEASURE ABBREVIATIONS USED IN THIS REPORT

Metric Units

dB	decibel	m	meter
h	hour	m/s^2	meter per second squared
Hz	hertz	min	minute
kHz	kilohertz	ms	millisecond
km	kilometer	s	second
km/s	kilometer per second	V	volt

U.S. Customary Units

ft	foot	g	acceleration of gravity
ft/s	foot per second		

Reference to specific products does not imply endorsement by the U.S. Bureau of Mines.

STUDIES OF STOPE-SCALE SEISMICITY IN A HARD-ROCK MINE

PART 1: METHODS AND FACTORS

By Robert L. Kranz,[1] John P. Coughlin,[2] and Selena Billington[1]

ABSTRACT

The U.S. Bureau of Mines (USBM) has been monitoring and studying seismic activity associated with mining in the Coeur d'Alene silver district of northern Idaho. New statistical methods of studying the stope-scale (1- to 100-m) seismicity at one Idaho silver mine are used in this report (part 1) and its companion (part 2). This report deals with methodology and its limitations. The recent concept of fractals and their seismological use is discussed and applied to mining-induced seismicity. Three types of fractal studies are addressed: spatial analyses (including temporal changes of spatial patterns), temporal analyses, and size analyses. Other statistical measures of mine seismicity are also addressed: event mean location, inter-event distance distribution skewness, temporal coefficient of variation, nearest neighbor and next event statistics, and event location planarity patterns. Each of the methodologies discussed (fractal and nonfractal) is presented using sample data from two stopes in the mine.

It is shown that stope-scale, mining-associated microseismicity has a fractal nature. The usefulness of demonstrating fractality (scale invariance) for predictive or descriptive purposes depends on recognition of the factors affecting the calculation of fractal dimensions. Several methodological traps are illustrated that can lead to an incorrect conclusion.

[1]Geophysicist.
[2]Electronics engineer.
Denver Research Center, U.S. Bureau of Mines, Denver, CO.

INTRODUCTION

For many years, as part of its mine safety program, the U.S. Bureau of Mines (USBM) has conducted studies of mining-induced and associated seismicity in hard-rock mines in northern Idaho (*1-5*).[3] In one mine (the Galena Mine), data have come from a mine-wide acoustic monitoring system operated in conjunction with ASARCO, Inc., the mine operator (*4*). The system has provided researchers with the opportunity to study the interrelationships among mining activities, geological structure, and associated stress changes (*5-14*). The information contained in the large amount of data collected over the years has not yet been fully utilized and remains a valuable resource for future analyses. In addition, a new digital network was recently installed in the mine, providing even more data and opportunity for understanding the complex mining environment.

This report (part 1) and its subsequent companion (part 2) use new statistical methods and data previously collected to study seismicity in the mine at the stope scale (1 to 100 m (3 to 328 ft)). The goals of the work are (1) to determine the characteristics of stope-scale, mining-associated, spatial and temporal seismicity patterns, (2) to distinguish, if possible, background, blasting, and rock-burst-associated seismicity, by their attributes, and (3) to assess the potential of using this information for the purposes of rock burst prediction and geological structure analysis. Part 1 deals explicitly with the methodology and its limitations. Data from two stopes in the mine are used to illustrate the analytical methods, make spatial and temporal comparisons with other real and artificial data, and demonstrate some significant interpretational problems. Part 2 describes the use of classification and pattern analyses of similar data covering longer calendar periods and more occurrences of rock bursts and blasting activity. In both parts, the terms "rock burst" and "bump" are used synonymously; the former usually connotes damage to the stope, in that rock has been ejected into the mine openings. The latter term is more encompassing, including nondamaging seismic disturbances within the rock mass large enough to be recorded at the surface.

Where appropriate, references are made to similar studies at both smaller scales (laboratory acoustic emissions) and larger scales (tectonic earthquakes). Indeed, *the hypothesis running through these studies is that mine seismicity has a fractal or self-similar nature that, if determined, can be useful in understanding its occurrence and relationship to rock fracture processes and geologic structure at all scales.* Accordingly, a major effort has been put into measuring spatial and temporal fractality, if it exists. This approach is currently in vogue in all physical sciences (*15-16*). In taking this approach, we do not imply that more traditional seismological analyses are less applicable or less useful in reaching our goals. We hope that any information extracted from the data in this way will be complementary, not contradictory, to that obtained using the more traditional methods.

[3]Italic numbers in parentheses refer to items in the list of references at the end of this report.

FRACTALS AND THEIR SEISMOLOGICAL USE

The word "*fractal*," used as a *noun*, refers to a set of points having a characteristic measure, called the fractal dimension, that meets certain mathematical criteria. The point set can represent a nonphysical collection of data, such as frequencies, but it usually represents a physical property of an object, such as length or mass. It is the set of points representing the object, not the object itself, that is properly called *a fractal* because the fractal dimension of the set strictly exceeds the topological dimension of the physical object. However, in common usage, to say something is a fractal simply means that it has a "shape made of parts similar to the whole in some way" (*15*). The word "*fractal*," used as an *adjective*, indicates explicitly the essential scale invariance and self-similarity of an object's property over the scale of observation of that property. The fractal property appears the same when examined at different scales. For example, the length of an object would be fractal if it is described by a power law dependency of the length upon the scale of observation (or ruler being used). To take another example, the density of particles in a dust cloud may be fractal if there is a power law relationship between the number of particles of a certain size counted in a volume and the magnitude of that volume. Such functional relationships described by power laws are self-similar because multiplying the independent variable by a constant (i.e., rescaling) will not change the functional relationship form, only the proportionality. The exponent in any such power law relationship is relatable to the fractal dimension that characterizes the property.

It is entirely possible that a fractal object (or set of points representing that object) may have different fractal dimensions for different properties (i.e., different properties scale differently). If fractality is different in different directions, the set of points is more properly described as *self-affine*. Although unlikely, if a fractal object has a single fractal dimension over all scales of observation, it is a *homogeneous fractal*. It is more likely that a fractal object has different fractal dimensions appropriate to different bounded, possibly overlapping, ranges of observational scale for the same property. It would then properly be called *multifractal*. Multifractality is, in essence, a distribution of fractal dimensions. The salient feature of fractals is, however, their self-similar character over a range of scales of observation or measurement.

Point patterns that do not actually represent physically contiguous objects can be examined at different scales of observation for their self-similar appearance in the same way that convoluted coastlines, dendritic diffusion patterns, and cloud shapes have been. As applied in the seismological context, seismic event locations can be considered as three-dimensional spatial point patterns, and the time of occurrence of seismic events as unidimensional time point patterns. In fact, since seismic events represent a five-dimensional point set (time, three spatial coordinates, and magnitude), any subset of these can be investigated for self-similarity. If, when examined at different scales, the patterns have a common characteristic measure, this simplifies the description as well as any analysis that looks for changes in the patterns for predictive purposes. In other words, showing that seismicity has a self-similar, scale-invariant measure (fractal dimension) over a range of spatial or temporal scales would provide a basis for understanding the process that gave rise to the seismicity and the opportunity, even without the understanding, to use that information to good purpose.

Several types of fractal dimensions have been used to quantify scale invariance. These are described in detail by Feder (*15*) and Korvin (*16*). Briefly, two of the more commonly measured fractal dimensions are the *capacity* dimension and the *correlation* dimension. One can determine a capacity dimension by counting the minimum number of boxes necessary to contain the point set as a function of the box size or the number of points in a spherical volume as a function of radius. One can determine a correlation dimension by counting the number of point pair distances less than a specific distance as a function of a range of distances. In both cases, if the functional dependency of count (or mass) on scale is a power law, the corresponding dimension is determined by the power law exponent. Log-log plots of the counts as a function of the scale parameter would then yield a straight line whose slope determines the fractal dimension. This dimension is also called a fractional dimension because it typically has a noninteger value, unless it corresponds to the limiting, whole-number topological dimension.

In the case of either the capacity or correlation dimension, the *degree of clustering* of the points is inversely related to the fractal dimension. If the points represent locations in space or event occurrence time, even random placements or occurrences may exhibit some clustering. Random positions that are homogenous at all scales will have fractal dimensions of 3.0 if volume filling, or 2.0 if plane filling. Deviations from such random positions by a set of seismic event hypocenters or epicenters can be measured by fractal dimensions less than 3 or less than 2, respectively. Lower fractal dimensions signify more spatial clustering. Temporal clustering of event occurrence times is exhibited by temporal fractal dimensions less than 1.0, which corresponds to uniform, random occurrences. Lower temporal fractal dimensions signify more isolated occurrence time groups. If the maxim "near things are more related than far things" applies to seismicity, then the fractal dimension might be useful for studying the *strength* of spatial and temporal associations.

The fractal nature of seismicity has been demonstrated for earthquakes occurring in a number of different regions of the earth, and over specific time periods (*17-25*). Kagan and Knopoff (*17*) defined a normalized two-point correlation integral (second-order moment) of inter-event distances and used it to study the distribution of distances between pairs of epicenters or hypocenters. They found that the number of event pair distances less than a specific distance scale displayed a power law dependence on that scale and so was spatially fractal. The scale invariance was different, however, for different catalogs. Sadovskiy and others (*18*) examined earthquake location probability (with aftershocks removed) as a function of regional area that was subdivided hierarchically into smaller and smaller portions. They determined that the relationship of above-average seismicity to the area containing the seismicity was self-similar, and calculated a capacity dimension. Ouchi and Uekawa (*19*), although never mentioning the word "fractal," nevertheless took a similar approach to that of Sadovskiy and others. They also found that clustering of events was greater than what would be expected from random spatial occurrences, and that this clustering had a self-similar character when examined over different areal subsets. De Rubeis and others (*20*) used the correlation integral to measure the spatial correlation dimension for seismic event pair distances in Italy. They then examined how that dimension changed in time within a fixed region, finding increases and decreases in fractal dimension related to major events. Hirata and Imoto (*21*) and Hirabayashi and others (*22*) studied spatial multifractality. There appeared to be no single, homogeneous fractal dimension for the catalogs studied, but somewhat different fractal dimensions at different scales. Smalley and others (*23*) applied the correlation integral to event time intervals to show that the temporal fractal nature of seismicity persisted over scales of several years in the New Hebrides. Similarly, Papadopoulis and Dedousis (*24*) showed that the scale-invariant temporal clustering of earthquakes held over long periods in the Hellenic arc-trench system. Kagan and Jackson (*25*) also employed a version of the two-point time correlation measurement to examine the statistical properties of several earthquake catalogs. They determined that the seismicity was temporally fractal and that long-term variation in seismicity was governed by a power law distribution.

Acoustic emissions (AE) from microcracking in laboratory rock samples have been shown to have spatial fractality (*26-28*). Hirata and others (*26*) found that AE

locations in rock creeping under constant deviatoric stress were spatially fractal with a correlation dimension that decreased as the failure time approached. Kusunose and others (*27*) showed that the fractal AE location distribution in large-grained granitic rock has a natural scale imposed upon it by the grain size of the rock. A different spatial correlation dimension was obtained for scales less than and greater than the mean grain size in the same rock. Kranz and others (*28*) measured both a correlation dimension and a capacity dimension for AE generated in deforming rock before and after raising borehole fluid pressure. They found a slight decrease in fractal dimensions after the rise in pore pressure, confirming increased event location clustering.

All of the above studies are relatively recent. However, long before the concept of fractality was introduced, seismologists had demonstrated the essential self-similarity of earthquake size distributions with the well-known and often since confirmed Gutenberg-Richter frequency-magnitude scale. The relationship between the "b-value" or exponent in this scaling law and the spatial fractal dimension of events has been examined recently (*29-32*). Discussion has centered around the fractal distributions of crack, fault, or asperity size and the corresponding AE or earthquake size. Clearly, the inverse problem of associating spatial fractal dimensions of seismicity with the size distribution of geologic structures to which they may be related is quite formidable without independent observations of those structures. Nevertheless, the scale invariance of event magnitude has important implications for both the physics of failure and the structure(s) that fails (*29-32*).

APPLICATION OF FRACTAL CONCEPTS TO MINE SEISMICITY

It is tempting to *assume* that since earthquakes and acoustic emissions have been shown to be fractal in time, space, and magnitude, such will be the case at the intermediate rock mass scales associated with mining. In this report we will demonstrate that this assumption is indeed true for at least this one particular hard-rock mine. However, as will be made apparent, there are difficulties in applying this information for predictive purposes because (1) data quality suffers from generic seismic network peculiarities and lack of knowledge about the rock mass, and (2) the mine is both artificially and tectonically stimulated simultaneously on overlapping, but poorly constrained temporal and spatial scales. However, we prefer to view these difficulties as opportunities to use the concepts of scale and fractality to help in understanding how these various artificial and natural factors interact and the limits they place on our abilities to predict rock bursts or infer structure based on seismicity.

There are a number of ways one can apply the seismological and laboratory experiences with fractality referenced above to aid understanding of mining-associated seismicity. These are complementary to more traditional statistical analyses of seismicity. First, one can look for temporal changes in fractal dimension at the same locality to see how they may be related to blasting and rock bursting that occur there. Traditionally, this has been the role played by studies of event rate (*8, 33-34*) or by studies of b-value changes (*35-36*), especially in the search for rock burst or earthquake precursors. Recently, using previously published USBM seismicity plots (*34*), Xie and Pariseau (*37*) claimed to have seen a 3-day decrease in spatial fractal dimension prior to a large bump in a coal mine. Eneva and Young (*38*) also claimed to have seen decreases in fractal dimension preceding large rock bursts in a Canadian nickel-copper mine. Confirmation of consistent changes in fractal dimension, independent of the various ways the fractal dimension could be derived, would prove useful for predicting rock bursts. Furthermore, because seismicity is a result of the complicated interaction between heterogeneous stress and strength distributions, demonstrations of no changes in seismic fractal dimension might indicate a lack of significant change in unmined rock mass strength. From laboratory experiments, decreases in b-value (a measure of fractality with regard to size) have been associated with increasing stress. This association has not always been confirmed in larger scale tests (*39*). Although in the mine environment most rock mass is not directly observable, concurrent mappable structure and seismicity data sets may exist and could be used to evaluate hypothetical associations among spatial fractal dimensions, b-values, induced stress changes, and geological structure changes.

Next, from the fractal dimension, one can compare the degree of temporal and spatial clustering between blasts, blast-associated bumps or bursts, and isolated rock bursts. One can compare the fractality between different stopes, possibly relating differences to structural features or mining practices. In particular, one can search for scale-bounded fractality as evidence for effects of structural features at different scales of interaction.

In summary, the application of fractal analysis methods to mine seismicity seems to offer much in the way of both ancillary information and information not obtainable otherwise. The following section describes the stopes, network, and data employed in this study, after which a description of methods, examples of results of the data analyses, and related cautions with respect to their use are presented.

DESCRIPTION OF STOPES, NETWORK, AND DATA

All microseismic data in this report were collected in the Galena Mine, located near Wallace, ID, in the Coeur d'Alene mining district. In this mine, the ore-bearing host rock is an argillaceous quartzite. The principal ore minerals are silver, lead, and copper occurring in near-vertical, imbricated veins striking northeast. Larger scale regional faults, through and around the mine, trend northwest with steep dips (*9*). To expose and extract the ore, individual stopes are extended upward along raises between mine levels that are typically 92 m (300 ft) apart. Stope dimensions vary according to the local extent of the vein, but typically, widths are 3.05 m (10 ft) and lengths on either side of the raise are 15.25 to 24.4 m (50 to 80 ft) with 61 m (200 ft) as a maximum. The long dimension of stopes is oriented along the strike of the ore-bearing vein in the immediate area. The rate of mining is typically one 2.4-m (8-ft) cut per month, taken by blasting face rounds placed in boreholes drilled 1.2 to 2.5 m (4 to 8 ft) deep. Figures 1 and 2 show stopes 307 and 189, respectively. As shown in these figures, the stopes are near-vertical cuts on either side of 92-m (300-ft) raises extending between the 4900 and 4600 mine levels where access drifts have been driven. All of the data presented in this report (part 1) come from the geophone networks encompassing these two stopes. Data presented in the companion report (part 2) come from these and other stopes.

These stopes are two of eight similar areas in the mine on a networked microseismic monitoring system. In each

Figure 1

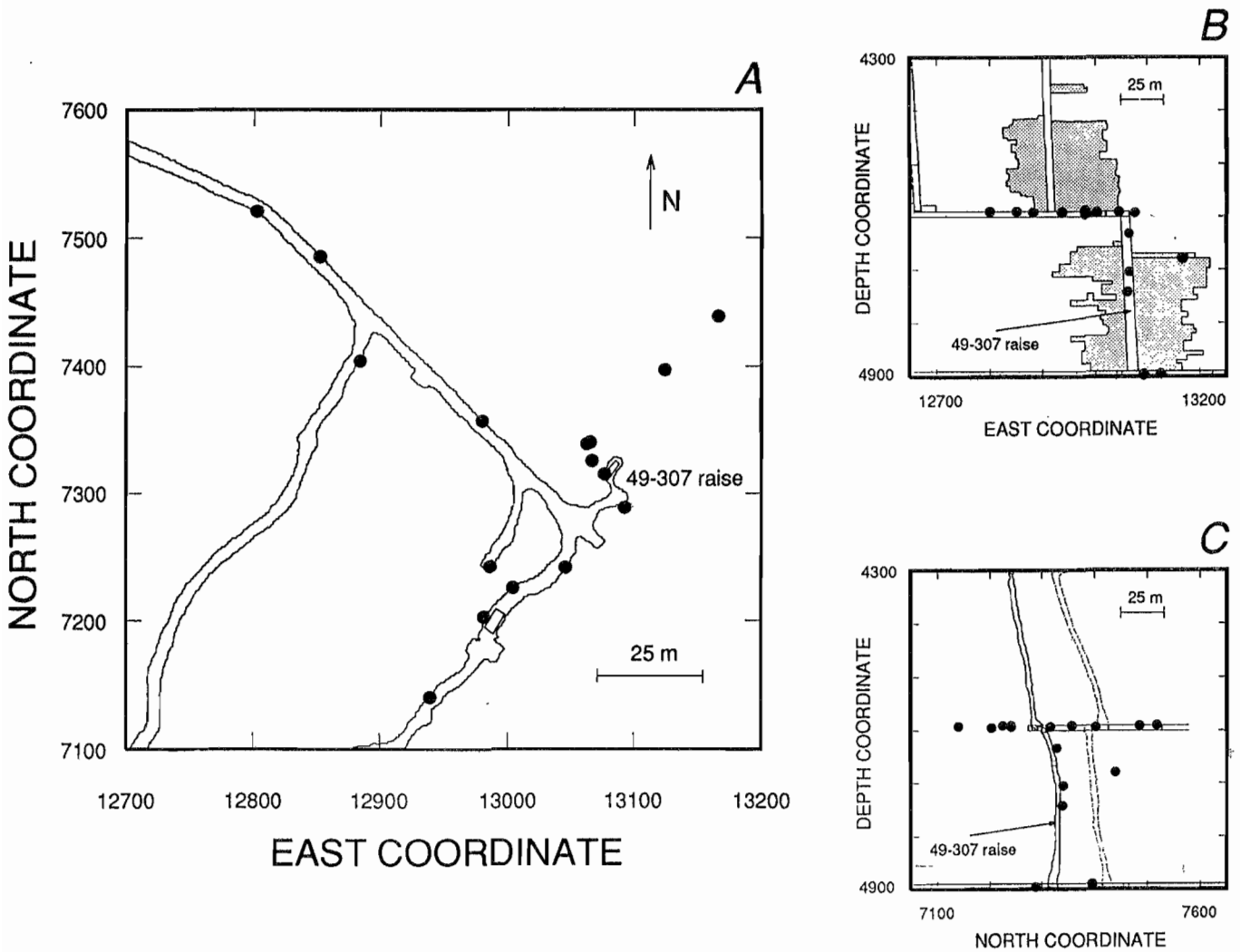

Galena Mine stope and raise 307. A, Plan view; B and C, cross sections. Symbols indicate geophone positions. Dimensional units are mine coordinates, in feet.

of these areas, an array of 16 accelerometers, surface-mounted in transecting drifts, raises, and crosscuts, has been connected by cable to a locally installed device called a "rock burst monitor" (RBM). The RBM detects microseismic events and transmits event data to a central network monitoring system via short-haul modem. Workstations on the network process the incoming data and, where the data are sufficient, calculate and display microseismic event locations. Apart from occasional interruptions due to unpredictable factors such as power outages or equipment failure, microseismic data are acquired around the clock.

The accelerometers are Wilcoxon amplified-output 793-M devices with 40 V/g output.[4] Frequency response is within 3 dB between 6 Hz and 6 kHz. Degradation of output signal due to cable length has been minimized by having data acquisition hardware installed in the monitored area. The RBM (custom built by Science Applications International Corp. according to USBM specifications) detects transient microseismic events by counting the number of accelerometer channels exceeding a given threshold in a set time window. Minimum channel count, threshold, and time window are all user adjustable. Triggering threshold, set on a per-channel basis in 0.2-V steps, ranges from 0.5 V to a maximum of 3.0 V. Time window may vary from 1 to 199.9 ms in 0.1-ms steps.

For each detected microseismic event, the RBM provides first-phase arrival times and data related to event energy. Arrival times, having a resolution of 0.1 ms, are measured for all triggered channels. A comparison with manually picked arrival times showed that the accuracy of

[4]Standard industry practice expresses accelerometer sensitivity in V/g, where g=9.80665 m/s^2.

Figure 2

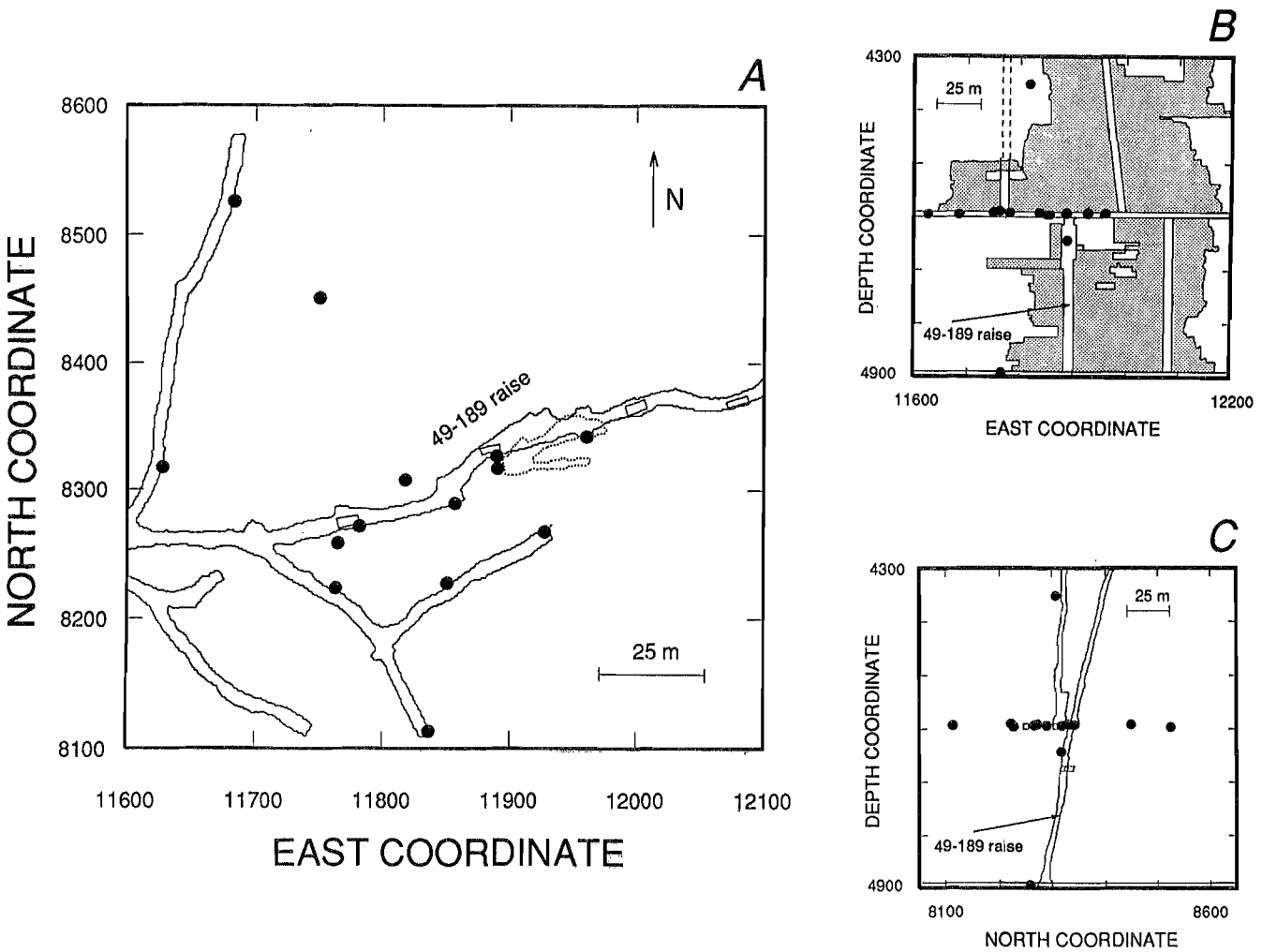

Galena Mine stope and raise 189. A, Plan view; B and C, cross sections. Symbols indicate geophone positions. Dimensional units are mine coordinates, in feet.

the automatically picked times was generally within 0.5 ms (*12*). Energy measurements are collected only for a fixed subset of four channels. On these channels, the input voltage is digitized at 40 kHz with 8-bit precision. These digital data are acquired during a time window that begins when any of the energy channels first triggers and ends according to a user-adjustable setting, up to 99.9 ms later. Energy is calculated by summing the squares of the voltage values within this time window. The relative energy value for each event reported by the RBM is then scaled to be a number between 1 and 12,000. *Digitized waveforms are not transmitted or archived with this system.*

The RBM is designed to work in a mining environment in which local noise such as drilling or air leaks may cause false triggers that could be interpreted as microseismic events. To remove this effect, the triggering threshold on each channel rises according to the length of time the channel remains above threshold.

Events are located with a direct least squares algorithm (*1-2*) based on a uniform average velocity of 5.64 km/s (18,500 ft/s). Channels having excessively late or impossible arrival times are excluded from the calculation. Event locations are checked for consistency with the input arrival times. This is done by comparing synthetic arrival times, derived from calculated locations, with the actual input arrival times. All channels except the first-hit and the second-hit channel must have arrival times that are positive and stand within designated ratio limits to the actual arrival times. The first-hit channel is necessarily excluded from the comparison since it provides the reference point; the second-hit channel is excluded from the requirement in order to avoid discarding locations that may be marginally closer to this phone than to the first-hit phone. The ratio limits are set through trial-and-error testing and calibration blasts. Event locations that have channels that exceed these ratio limits are of poor quality and therefore are not part of the spatial data sets examined in this report. All the data in both the part 1 and part 2 reports are considered to be "best quality" possible, within the limitations of the location program used (*2*).

Different stopes in this mine have significantly different ratios of "well-located" events to detected events; about 20% for stope 189, 10% for stope 307, and 37% for stope 99. For example, from July 1, 1989, to September 1, 1989, 105,248 events were detected in stope 189. Of these, 19,310 (or 18.3%) were best quality locations. In the same period, the stope 307 network detected 90,248 events with 6,604 (or 7.3%) best quality locations. The likely reasons for this discrepancy between stopes are more or less favorable distributions of geophone location sites on competent rock, and more or less damage in the stope regions. As the number of detected events greatly exceeds the number of well-located events, the set of event times may more accurately represent stope-scale seismicity in a statistical sense than the set of event locations.

A separate study (*12-13*) examined the accuracy and precision of event locations obtained using the RBM system at stope 99 in the Galena Mine. That study used a slightly less stringent definition of "well-located" than this study, and the primary conclusions were that (1) the location precision could be ±1 m (±3 ft), limited by the precision of the first arrival time picks, (2) the accuracy might be ±10 m (±33 ft) primarily as a result of inadequate modeling of the velocity structure, and (3) spatial variations in the apparent velocity exceeded 50% largely because of velocity reductions associated with fractured rock surrounding mine openings. The greatest component in error was in the vertical direction, owing to poorer station coverage between access levels.

SPATIAL FRACTAL ANALYSIS OF MINE SEISMICITY

In this report, spatial fractality is investigated using calculations of the two-point correlation integral:

$$C(R) = \frac{2}{n(n-1)} N(r<R), \qquad (1)$$

where n is the total number of points in the data set, and N is the cumulative number of location point pairs (X_i,X_j) having an interpoint distance r less than some scale length R. This means that in any data set of X_n event location points, *all* possible inter-event distances are calculated and used to determine the distribution. The log of C(R) is then fit as a function of log R, using traditional least squares methods. A power law is indicated if the fit is linear. Quality of the fit is also calculated. If C(R) is a power function of R, the slope of the best fit line to the data plotted in log C(R), log R space will give the correlation dimension, D. This is the method used by most investigators who have calculated correlation dimensions of point data, although the premultiplier normalization factor may vary somewhat. Kagan and Knopoff (*17*) actually normalized their measure to the same measure of an equal number of events randomly located in the same volume or area as the real data; they were determining deviation from random clustering.

Figure 3 shows three sets of location data for the same stope, one being a uniform random distribution created for comparison. Although only the x and y coordinates are plotted here in mine coordinates, the data analyzed actually contained all three spatial coordinates. Data were analyzed using equation 1. The results are shown in figure 4. The data are log-log linear, thus indicating a power

Figure 3

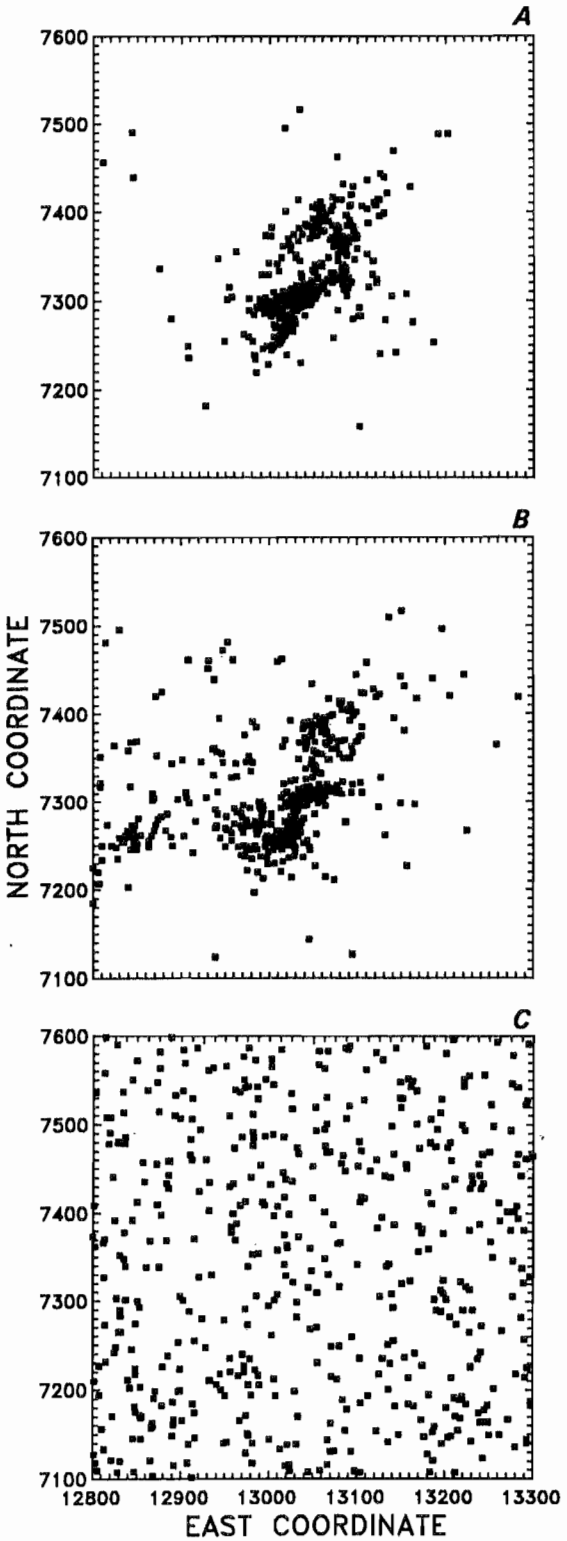

Epicenters for seismicity experienced in the Galena Mine near stope 307 during a few days time. A, July 1989; B, January 1990; C, artificial random seismicity centered on stope.

Figure 4

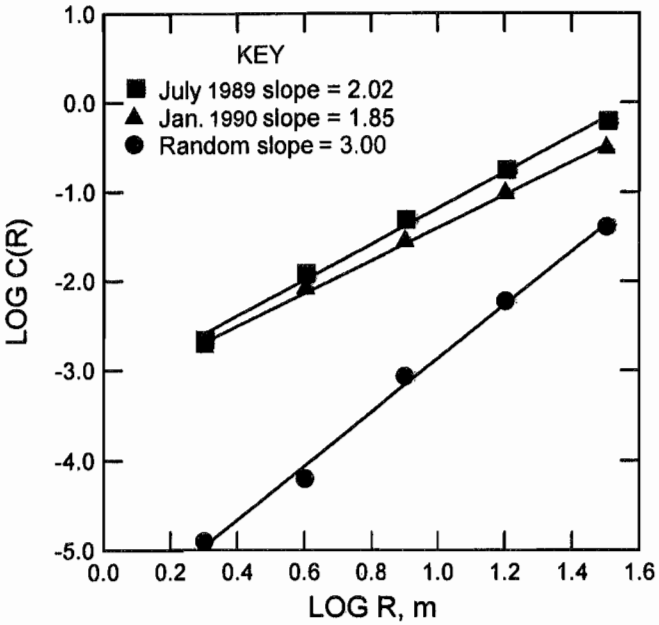

Correlation integral values as a function of scale; given slopes are corresponding correlation dimensions.

law relation and fractality. The slope is essentially the correlation dimension. Not shown in figure 4 are values for R greater than $10^{1.5}$ m. At larger scales, the well-known boundary effect causes rolloff from the straight-line projection. It is important to recognize this effect in the analyzed data and not extend the fitted line to greater than about half of the maximum inter-event distance, nor to less than about twice the minimum inter-event distance. As noted above, the lower the fractal dimension, the greater the degree of clustering. It is thus a quantification of what one sees qualitatively when comparing figures 3*A* and 3*B* with 3*C*. Although it may not be apparent from the figures that the January data are slightly more clustered than the July data, as indicated by their slopes in figure 4, this is only because the depth dimension is not shown in figure 3.

A note of caution is in order here. Slopes of lines can typically be fit to several decimal places. The uncertainty of the data would make further resolution superfluous and could lead to unwarranted conclusions concerning differences in slope between data sets. Fractal dimensions determined from fitting lines to data in log-log space are seldom accompanied by the uncertainty associated with the fit, although correlation coefficients may be given. It has been our experience that unless the correlation coefficients (R^2 values) are 0.97 or better, the assumption of linearity and reporting of fractal dimension to greater than two decimal places is very questionable. Criteria have also been proposed (*40*) for the minimum number of analyzed

point pairs necessary to achieve a high degree of confidence in any correlation dimension. The data sets analyzed in figure 4 actually contain too few points to be 95% certain that the well-determined slope is truly the correlation dimension. Therefore, the stated values are technically only estimates of the fractal dimension. Nevertheless, in figure 4, it is clear that there is a significant difference in slope between both of the real location data sets and the random set.

It is important to keep in mind that the correlation integral is normalized by the number of events in the data set (compare equation 1). When two or more data subsets containing different numbers of points are analyzed and the results displayed on the same log C(R)-log R graph for the purpose of comparison, the absolute magnitude of C(R) at any scale is a proportionate value. Only the slopes of lines fitted to the data, or the related fractal dimensions, can be compared in an absolute sense.

It is not hard to show that isotropic, homogeneous, random errors in event location will not affect the calculation of the correlation dimension as defined above. However, as a result of the relatively poor control of the depth or z coordinate for the event locations used here, the location error is typically not isotropic. In addition, events near or beyond the boundary of the geophone net will have a different location error than events well within the network, so the error is also not homogeneous. We have not made a systematic study of the effect of these anisotropic and heterogeneous location errors on the correlation dimension, since the magnitude of these errors is poorly known.

A more encompassing problem is the potential difference between epicentral and hypocentral distributions. Many seismological studies in the literature have dealt only with epicentral data. If we ignore the more error-prone depth component and work only with the horizontal positions, how do the measures of fractality compare? To illustrate the nature of the problem, figure 5 shows a comparison of the application of the correlation integral to event locations with three spatial coordinates (hypocenters) as well as to the same locations with only two of those coordinates (epicenters). Figure 5 also shows the rolloffs at larger scales due to the boundary effect. In figure 5*A*, a synthetic set of homogeneous random locations has a correlation dimension of 2.88±0.05 when all three coordinates are used and 1.95±0.05 when only the x and y location coordinates are used. These values are slightly less than the theoretically appropriate values of 3.0 and 2.0, but they differ approximately by the expected value of 1 when homogeneous three-dimensional data are compared with the corresponding two-dimensional data.

In contrast, for real locations with their attendant errors, the situation can be more complex. Figure 5*B* shows analyses for both a set of hypocentral and the corresponding epicentral data. Note that the epicenter

Figure 5

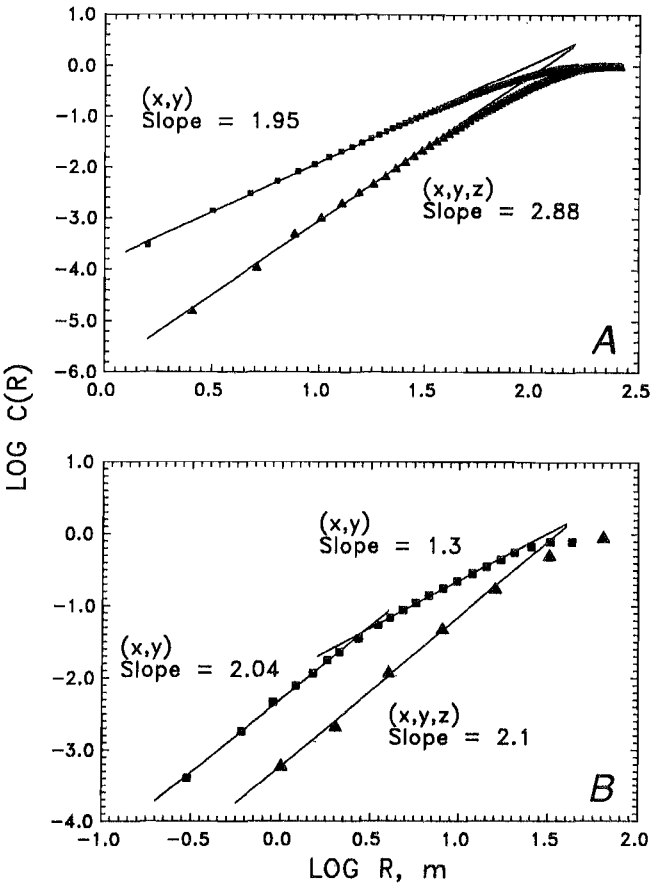

Correlation integral values for hypocenters (x,y,z coordinates) and epicenters (x,y coordinates). A, For synthetic, homogeneous random data; B, for stope 307, July 1989 data.

(x,y) data indicate that there is not a single log-log linear relation over the same linear range as the hypocenter (x,y,z) data. At least two different correlation dimensions, over different scale ranges, seem appropriate. Note also that although there are, as expected, proportionately more small-scale distances between epicenter pairs than between hypocenter pairs, the epicenter correlation dimension and the hypocenter correlation dimension are essentially the same over scales less than about 3 m (10 ft). Differences in the correlation dimensions do not appear until pair distances greater than about 3 m. This equality in hypocentral and epicentral correlation dimension is not plausible unless somehow the epicenters are randomly distributed at small scales, while at the same scales the hypocenters cluster. Beyond the 3-m scale boundary, there is a difference of 0.8 between the correlation dimensions. As indicated above, it should be a difference of about 1.0, if epicenters and hypocenters share the same degree of clustering, i.e., if the location point set is homogenous.

This is not a unique case. More often than not, correlation dimensions for real hypocenters and corresponding epicenters differ by less than unity (some differences are as low as 0.35). Event hypocenters on one or more steeply dipping planes might appear less clustered in three dimensions than when projected onto any intersecting horizontal plane. At this time, we cannot say how much of this effect is due to the larger uncertainty in the z coordinate, or whether there is a structural explanation for it. Based on our experience, we caution against assuming that fractal epicenter and hypocenter point patterns differ simply by a value of 1 in fractal dimension.

One of our goals is to be able to distinguish blasts from bumps through analysis of the seismicity. Figure 6 shows an event rate plot for a 5-day sequence. Shown are the rate increases associated with a production blast and a large double bump the next day. Generally, one cannot rely solely on event numbers or rates to make distinctions, since they depend heavily on blast size. Here the event rate decay pattern is clearly different for the blast and the bumps, but what about the organization of event locations? Figure 7 shows the results of analyzing the event locations after the blast and after the double bump. Over the same range of spatial scale, the postblast seismicity has a higher correlation dimension than the postbumps seismicity. This means the postbumps seismicity was more clustered than events following the blast. Unfortunately, such a clear distinction cannot always be made between blast and bump aftershock sequences. This will be discussed further in the part 2 report.

Suppose we divide the data set just discussed by "size." In general, one may want to do this to study only large events, since they have more damage potential. In practice, one way to do this is by choosing events that produced above-threshold signals on more than or fewer than a certain number of geophones in the local network. How would that affect the spatial correlation dimension calculated? Figure 8 shows the results of such an exercise. The subset that includes only the largest events, having at least 15 out of 16 geophones triggered, does not display the same slope at the lower scale range (below 10 m) as events that triggered at least 9 geophones. Since the latter subset includes the events in the former subset, one interpretation is that the locations of large events were not similarly distributed below some inter-event distance. There were proportionately more clustered large events with locations closer than 10 m to each other than would be expected from the correlation dimension calculated using the bigger data set. An explanation for this observation might be that the large aftershocks tended to occur near the progenitors, and therefore near each other, while smaller events were more distributed throughout the network area. In general, one can expect that any perceived scale boundary in data censored or filtered by event size will be a function of the event size considered. Subsets containing only larger events may have different calculated fractal dimensions than data sets containing more numerous, but smaller size events. For comparative purposes, data sets should contain events with the same lower size limit.

Figure 6

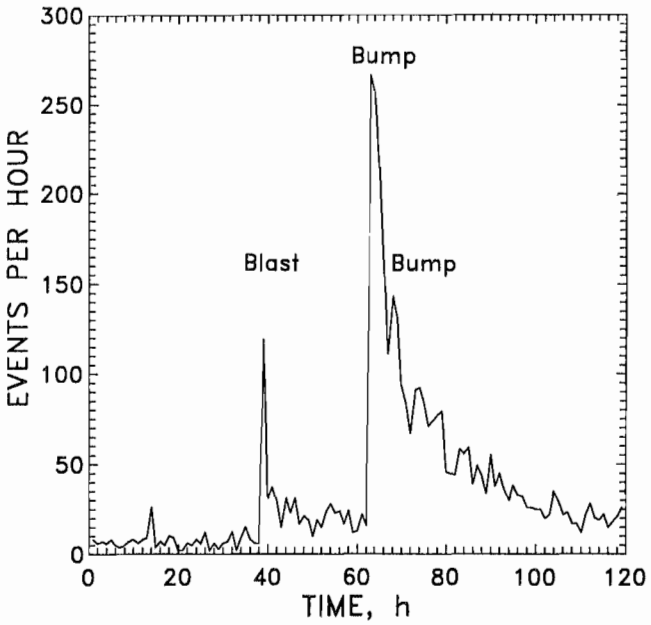

Event rate as a function of time following production blast and large double bump in March 1990, stope 189.

Figure 7

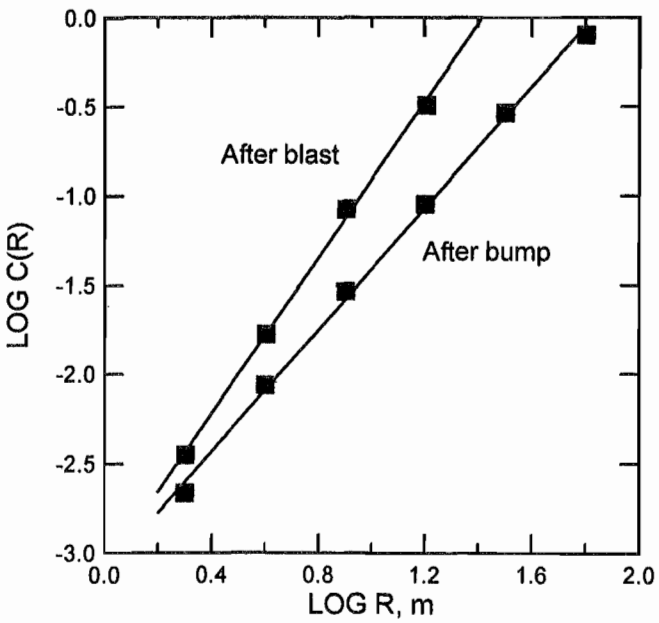

Comparison of correlation integral values for postblast and postbump time periods shown in figure 6. Correlation dimensions are 2.25 and 1.70, respectively.

Figure 9 shows 19,310 events located during a 2-month period at one stope. Analyzing these points using equation 1 produces the results shown in figure 10. Clearly, *it would be incorrect to try to fit a single straight line over the entire distance scale range*. Instead, two straight lines are used, each fitting over only a portion of the scale. Note also the rolloff at larger scales due to boundary effects. If many more log C(R), log R points were plotted on the graph, one might be tempted to fit many more shorter straight lines to the data. We have, therefore, a conundrum: if the data are clearly not simply linear over the entire range of investigation, how do we determine the appropriate scale boundaries for a single correlation dimension? Scale boundaries are often interpreted to coincide with the scale of known geologic structures (*21-22, 27*) such as grain or plate boundaries. Here is an opportunity to identify structural scale in the mine. For example, one interpretation of the linear fits shown in figure 10, could be that the seismicity is being affected by some natural or artificial factor with a scale of about 6 m or less. Below this scale boundary, events are less clustered than on the scale of 6 to 40 m. In the absence of any identifiable geologic structure at that scale, another interpretation could be that the scale break is associated with a bimodal size distribution of seismic progenitors, such as small-scale blasts and larger scale bumps, that create overlapping but different location distributions. Still another possible explanation is that location error is about 6 m, and this somehow results in fewer than expected locations closer than 6 m from other locations. At this time, there is no objective method of evaluating which of these explanations is most likely in the mine, but it is a research topic we are pursuing.

Figure 9

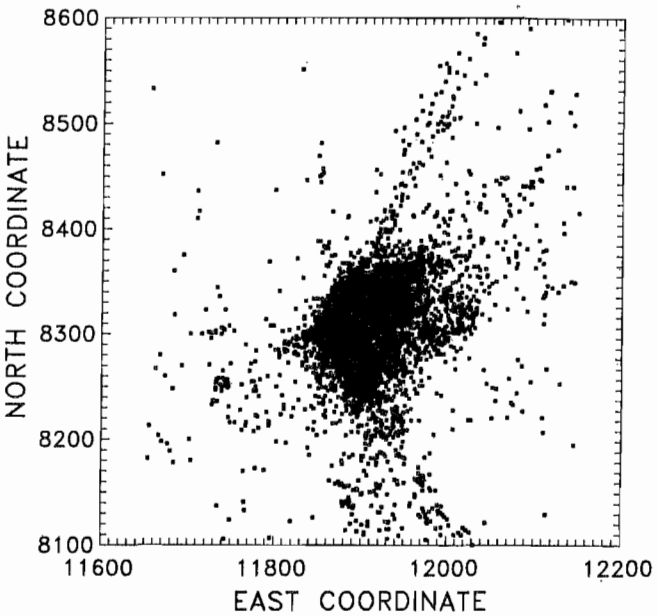

Epicenters of 19,310 events located during July and August 1989 at stope 189.

Figure 8

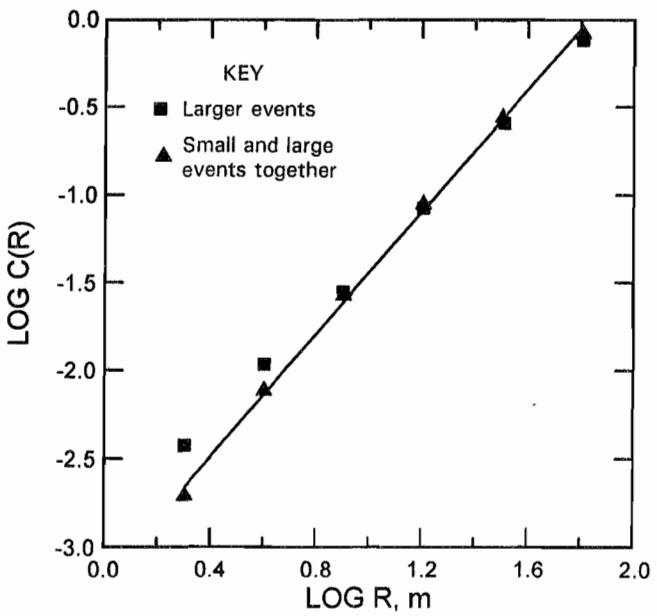

Values of correlation integral for two subsets of event locations after initial bump shown in figure 6. Triangles: data for all events over threshold on nine or more geophones. Squares: data for all events over threshold on at least 15 geophones.

Figure 10

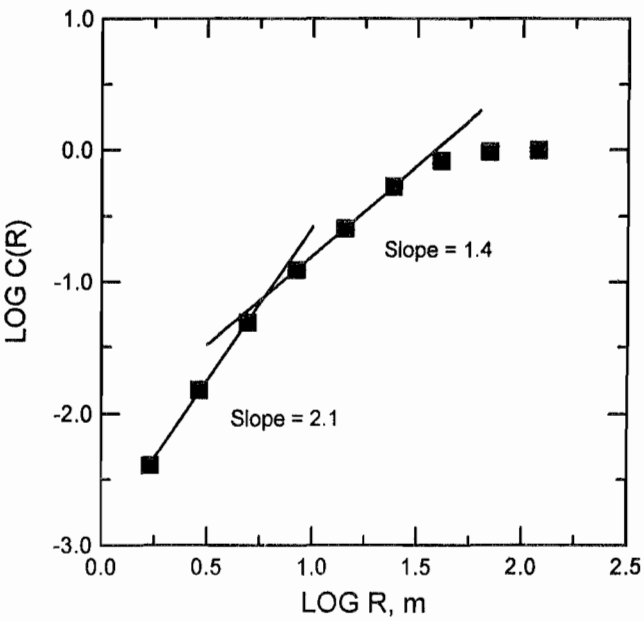

Correlation integral values for all data in figure 9.

TEMPORAL ASPECTS OF SPATIAL FRACTALITY

Figure 11 shows the detected event rate changes during the same 2-month period shown in figure 9. The significant production blasts and bumps associated with some of the rate peaks are identified in the figure. A natural, but surprisingly difficult question is "How does the spatial fractality change during this timeframe?" If it does change, are the changes associated with the significant blasts and bumps? More importantly, are there precursory changes in the spatial fractality that might be used to predict the bumps? The reason these are difficult questions is illustrated in the following sequence of figures.

Figure 12 shows the correlation dimension data in daily time windows and in equal event number windows. We chose daily partitions since mine work typically occurs on a daily schedule. There is no similar resonance in located event numbers. There are significant differences in these two plots. Although both show a similar mean value, the time-windowed data show greater deviations than the number-windowed data. The number-windowed data are preferred for the following reasons. First, the spikes in the number-windowed data are more easily associated with actual occurrences, such as periods of continuous mining work (days 4 to 8) or large bumps (days 34 and 35) that are not as obvious in the time-windowed data. The large spike during days 58 and 59 in the time data cannot be associated with any natural or artificial activity in the stope, and is therefore likely to be an artifact of the window partitioning. Second, each point in the time-windowed data is derived from different daily numbers of events: as few as 200 to as many as 1,200. Previous studies have shown that there is less uncertainty in the derived correlation dimension when larger numbers of points are used. There is a minimum number of points required to attain a reliable estimate of the true correlation dimension. Using the criteria proposed by Smith (*40*), if the scale of invariance spans one order of magnitude in three-dimensional space, we would need approximately 3,000 points to be 90% certain that we have the correct correlation dimension. Having less than 1,000 points decreases the accuracy to less than 75% certainty. Waiting for enough events to occur and be located may be impractical. Thus the extra noise in the time-windowed data may simply be due to the extra uncertainty associated with the less active days.

In the above example, did we fortuitously choose good or bad window partitions? We have looked through the time-windowed data with different partitions (such as from 3 a.m. to 3 a.m. instead of midnight to midnight) and with different periods. The correlation dimension deviations are always larger for time-windowed data than for similar

Figure 11

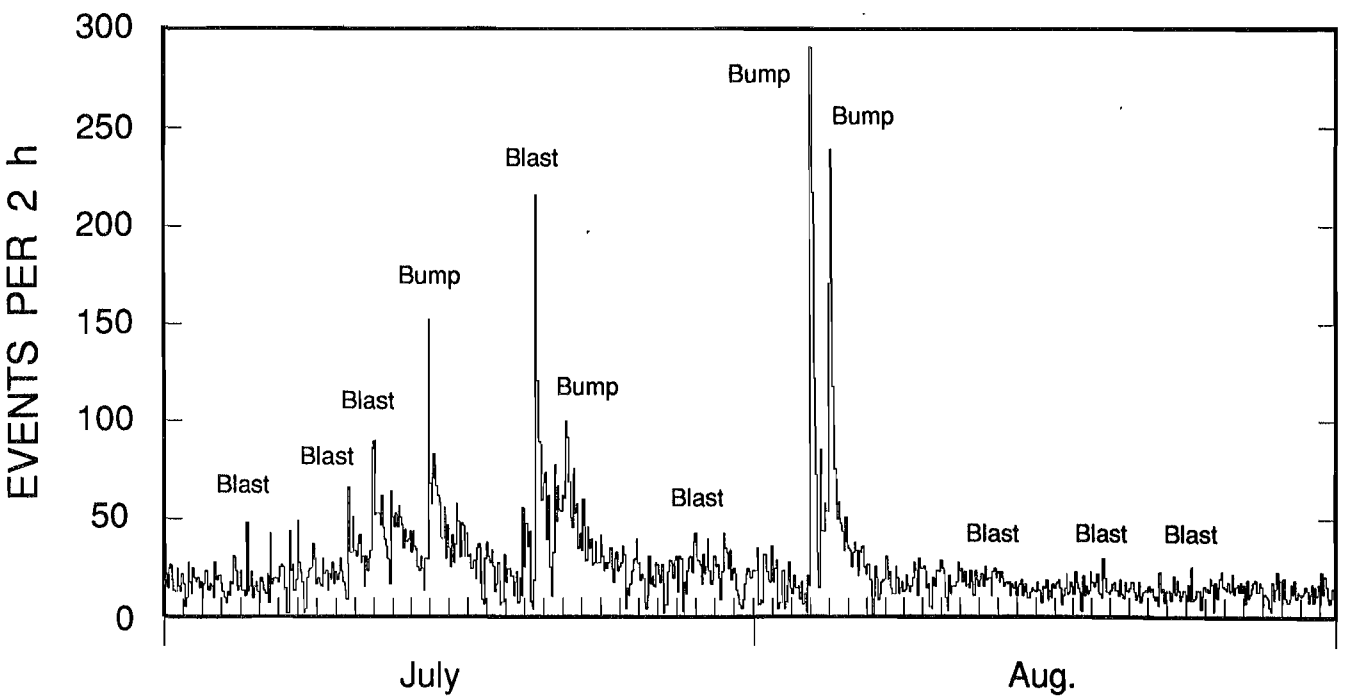

Event rates for July and August 1989 at stope 189. Two large rock bursts or bumps occurred approximately 24 h apart on August 4 and 5. Other significant peaks correspond to production blasts or smaller bumps.

number-windowed data, and harder to associate with real activity. Again, this may be because of the variability in numbers of events per time window. Well then, what about the effect of number-window size and overlap? These parameters also affect the information content of the time-varying correlation dimension signal. Figure 13 shows different window sizes, with different overlaps (same event numbers analyzed in successive windows), but with always the same overlap proportion. Both the resolution and fidelity of the deviations are clearly affected by the choices in these parameters. There should be an optimum number-window size that could be found for each stope, for use of the time-varying correlation dimension as a precursory signal with a prescribed accuracy.

Since lower dimension indicates greater clustering, we might want to test the hypothesis that spatial clustering increases before a major rock burst or bump by looking for decreases in correlation dimension. In figure 14 the previous figures are enlarged to include only 5 days before and after the two large bumps on days 34 and 35. In all figures, sharp decreases in dimension immediately *after* each bump reflect the fact that aftershocks tend to strongly cluster spatially. Starting on about day 31, an *increase* in correlation dimension is apparent in figures 14*A* and 14*B*, while no significant change is identifiable in figures 14*C* and 14*D*. Thus, it is clear that *attempts to find precursory spatial clustering by looking at changes in fractality will be highly dependent on the window parameters chosen.*

Figure 12

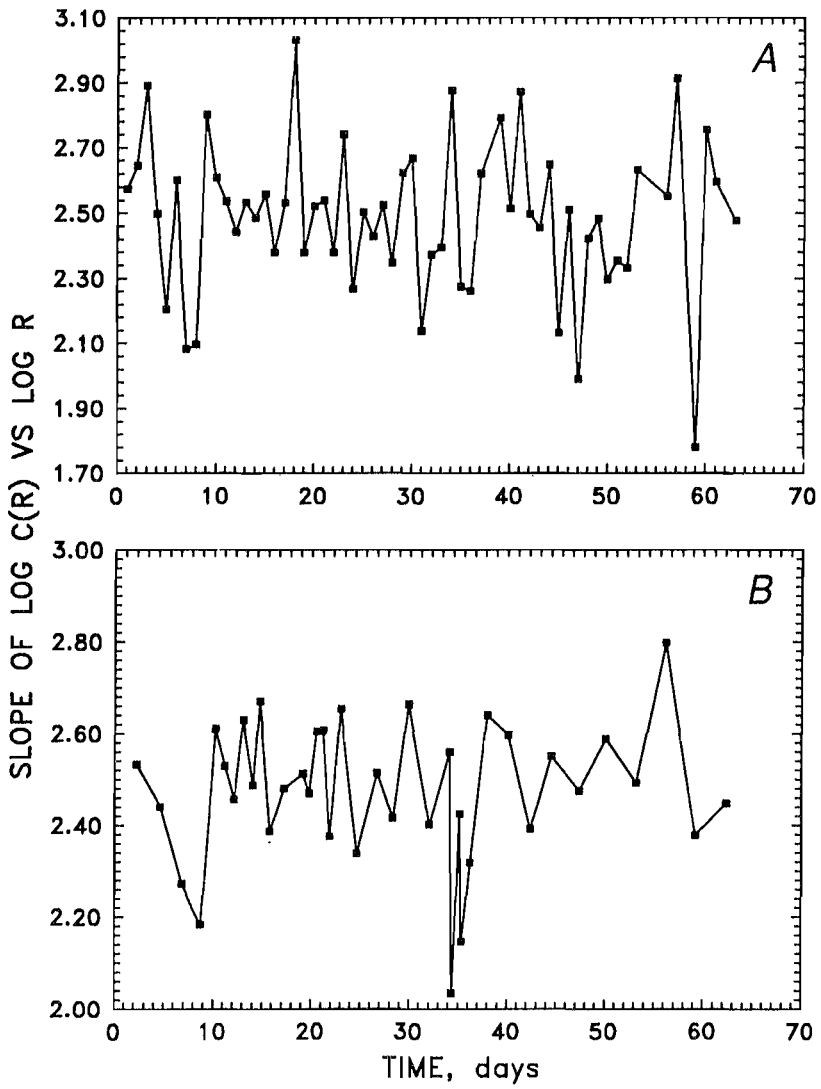

Slope of log C(R) versus log R correlation integral data subsets for (A) 24-h periods and (B) blocks of 500 events during the 2 months shown in figure 11. Numerical values on y axis are equivalent to fractal correlation dimension.

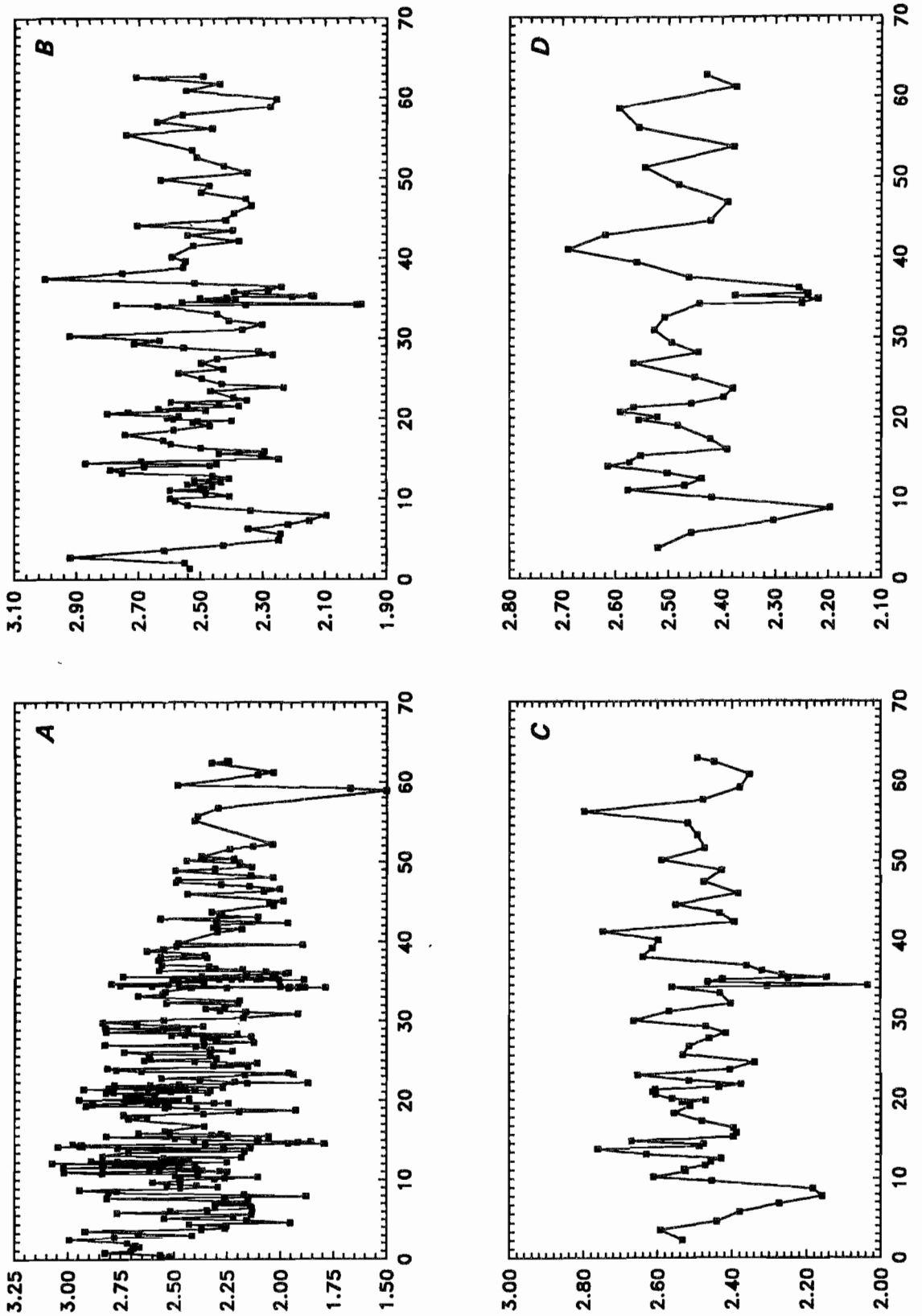

Figure 13

Slope of log C(R) versus log R for different numbers of events in each window with different overlaps (events used in successive windows). Similar to results in figure 12. A, 100 events with 50-event overlaps; B, 300 events with 150-event overlaps; C, 500 events with 250-event overlaps; D, 800 events with 400-event overlaps. Uncertainty in linear fit for each slope value is typically ±0.1 for less than 500-event blocks and ±0.05 for 800-event blocks.

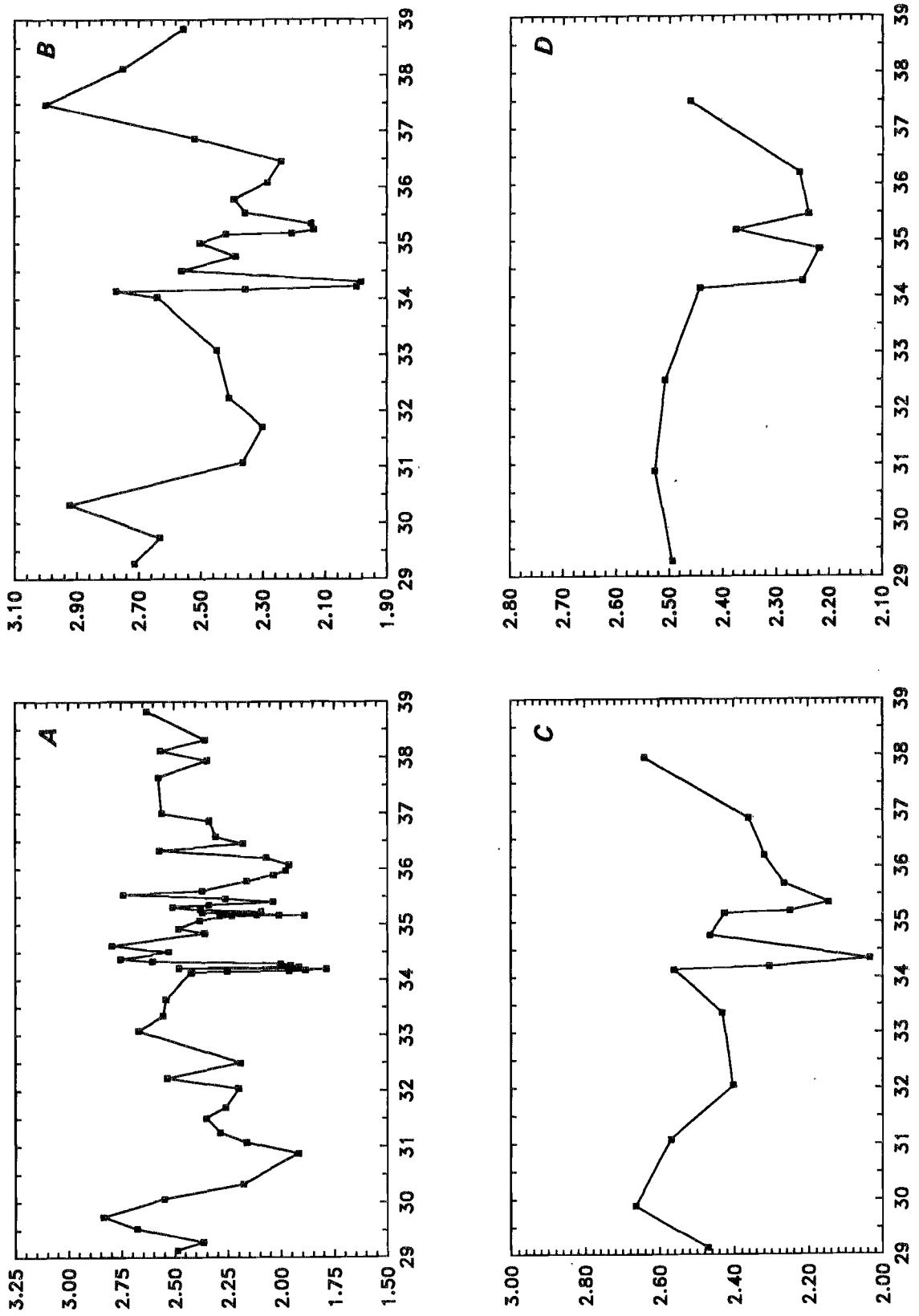

Figure 14

Expanded data from figure 13, to emphasize 5 days before and after the two large rock bursts on days 34 and 35. A, 100 events with 50-event overlaps; B, 300 events with 150-event overlaps; C, 500 events with 250-event overlaps; D, 800 events with 400-event overlaps. Uncertainty in linear fit for each slope value is typically ±0.1 for less than 500-event blocks and ±0.05 for 800-event blocks.

TEMPORAL FRACTAL ANALYSIS OF MINE SEISMICITY

If occurrence time interval is used instead of distance, for the variable in equation 1, we can examine the fractality of the event occurrence time distribution. That is, we define a temporal two-point correlation dimension by calculating

$$C(T) = \frac{2}{n(n-1)} N(t<T). \qquad (2)$$

In this case, N(t<T) is the number of event pairs separated in time by an amount, t, less than a time interval scale T. With this formulation, the slope of the line in log C(T), log T space is equal to D, where D is the temporal correlation dimension (*25*). Similar to the spatial correlation analysis, lesser slopes yield smaller fractal dimensions, indicating more isolated clustering in time. A Poisson process that produces a random sequence of events will have a temporal fractal dimension of 1.0, or a slope of 1.0 on a log-log plot of C(T) versus log T (*23, 25*). Note that Smalley and others (*23*) give a slightly different formalism, and Kagan and Jackson (*25*) further normalize the correlation integral by the maximum period T of the catalog of event times.

Figure 15 gives an example of the analysis for a temporally clustered sequence of events for 2 h following a large rock burst and the subsequent period of 2 to 14 h following the same event. Note the difference in slope of the best fitted lines: 0.78±0.02 for the first 2 h and 0.94±0.02 for the following period. This indicates a lower fractal dimension and more clustered grouping of event occurrences soon after the rock burst, but a less clustered, almost random event occurrence grouping later. Since the *rate* of occurrences in aftershock sequences generally decreases with time after the progenitor, we might hypothesize some sort of an inverse relationship between the temporal fractal dimension and the event rate. This will be explored further in the part 2 report.

Figure 15

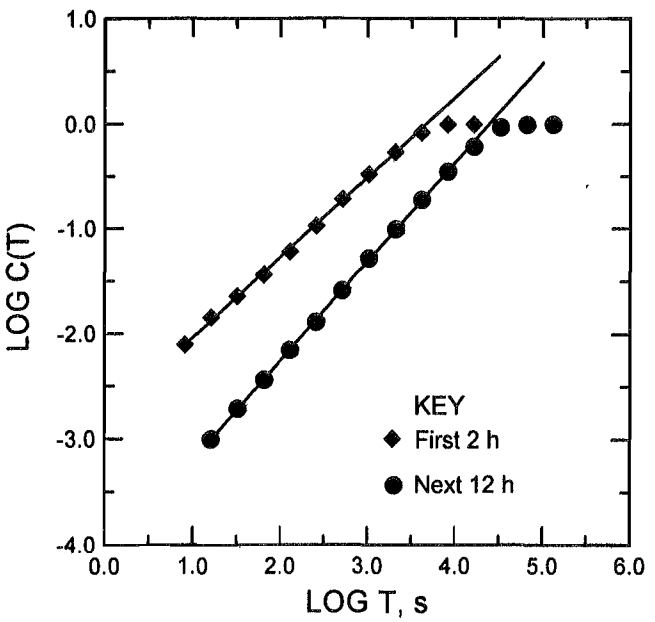

Time correlation integral data for two time periods (first 2 h and subsequent 12 h) after a rock burst. Slopes of best fitted lines are 0.78±0.02 and 0.94±0.02, respectively.

We can examine longer time series that include many aftershock sequences as well as less temporally clustered events to get a feeling for long-term fractality. Returning to the time data shown in figure 11, equation 2 is used to assess the temporal fractality for the first 34 days, up to the first of the large bumps. This time period encompasses a fair number of both production blasts and small bumps. Over 372 million time intervals were used. Figure 16*A* shows the results for the first 10 days and for all 34 days. The slopes of the lines are given. Several things should be noted. First, the data are fractal, but there appears to be a scale boundary at about $10^{1.7}$ (i.e., 50) s. Next, event pair time intervals shorter than about 1 min are much more clustered than longer time intervals. Interevent times larger than about 1 min are closer to being random. Third, the data for the first 10 days show a similar fractality as the data for all 34 days. That is, the long-term fractality is stable. Fourth, the longer data set displays a constant fractal dimension over at least four orders of magnitude in time. Since 10^6 s is more than 11 days, the implication is that occurrence times of events 11 days apart are distributed similarly to occurrence times of events only hours apart. After the double bumps, temporal fractality is maintained (figure 16*B*) over a comparable month-long period. These observations are examined further in the discussion section below.

What is the effect of censoring the data to include only the largest events in the series? Are they distributed similarly, and are they therefore a valid representation of the entire data set? Figure 17 shows the analysis for only the largest 10% of the events considered in figure 16, along with the data from figure 16*A* for comparison. The effect is similar to that for the censored spatial data. That is, the larger events are not distributed the same way at smaller time interval scales than most other events. Large events occurring closely in time are sparse, but large events that occur more than $10^{2.8}$ s (about 10 min) after other large events are fractally distributed in the same way as all the other event occurrences. Again, a boundary time scale could be defined for certain size events, below which a single temporal correlation dimension could not be determined.

Figure 16

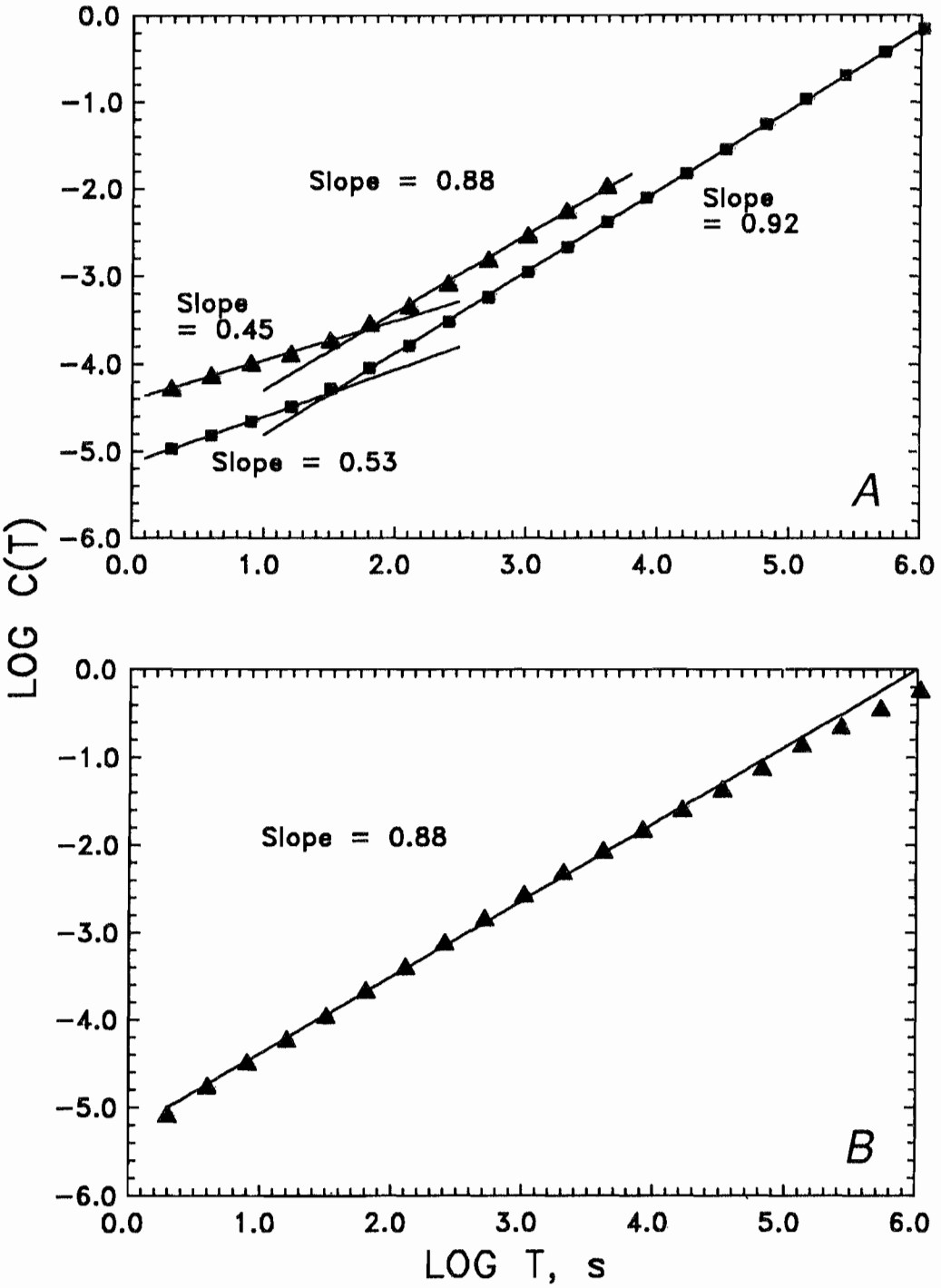

Time correlation integral data for various time periods. A, 34 days preceding August 4 rock burst in stope 189. Upper lines through triangles are for events occurring during the period July 1 through July 11. Lower lines through squares are for all 34 days. Error in slope is about ±0.02 so difference between lines is insignificant except at time scales less than about 1 min. B, Same analysis for comparable period of postburst time.

Figure 17

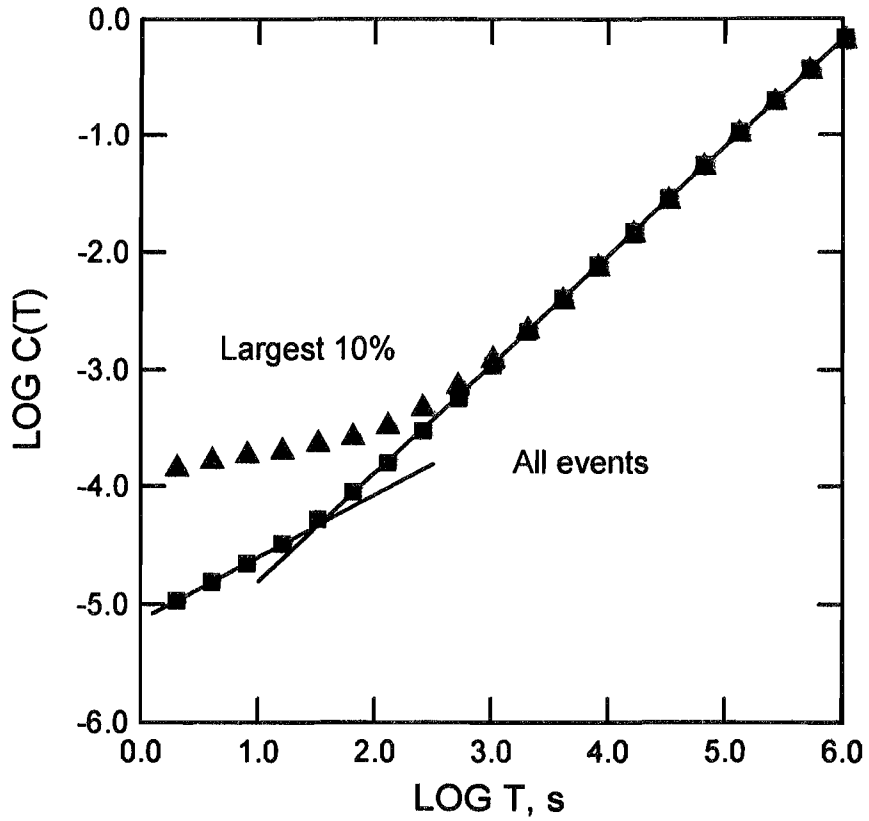

Comparison of time correlation integral data for two data sets: largest 10% of events (triangles) in comparison with all data in figure 16A (squares). Deviation from similarity occurs at about 10 min.

SIZE FRACTAL ANALYSIS OF MINE SEISMICITY

The correlation dimension for event size can be determined from the b-value in the Gutenberg-Richter frequency-magnitude relationship:

$$\text{Log } N = a + b \cdot M, \qquad (3)$$

where N is the number of events having a magnitude M *or less*, and a and b are fitted constants for a specified range of M values. Seismological magnitude M is typically corrected to account for such things as geometrical wave spreading, attenuation, and site coupling effects. Information about attenuation near or around each stope was not available and so was not considered. Magnitudes for blasts and stope-scale events derived from calibrated surface seismographs were too few to be useful. Attempts to use the number of overthreshold geophones for the calculation of the constants in equation 3 were generally unsuccessful. We had some success, however, in using "normalized energy" count. Since the magnitude M has been found to be proportional to the log of the seismic energy liberated, equation 3 can be rewritten as

$$\text{Log } N = A + B \cdot \log (E), \qquad (4)$$

where E is the normalized energy count, and A and B are fitted constants. To calculate a normalized energy, the raw

energy counts for each channel used in the event location scheme were first multiplied by the square of the distance between the corresponding geophone and the event location. These numbers were then averaged over the number of channels used. This procedure primarily accounts for geometrical spreading effects. In this formulation, B, taken as the b-value, is the slope of a log N, log E plot and can, in principle, be related to the size correlation dimension. Figure 18 shows one of the better fits to such data. Almost all of the b-values so obtained fall between 0.5 and 2.0 for the aftershock sequences examined so far and are, therefore, comparable to results for earthquakes. Attempts to use b-values for predictive purposes have all the same problems and conditions illustrated above for spatial and temporal correlation dimension determinations. Additionally, on average, there is a higher uncertainty associated with each b-value determination than with either the temporal or spatial correlation dimensions, since the determination includes errors associated with the energy-normalizing procedure as well as errors in slope calculation. This further lowers the usefulness of b-value changes, especially if those changes are small. For example, typical variations in b-value during the 16 h before and following a large bump are 0.2 to 0.4, about the same as the uncertainty in any one value. Some data sets do not appear to be fractal in size, no power law relationship being evident. We believe this can be attributed to problems with the original energy count determinations or the event locations in many cases.

Figure 18

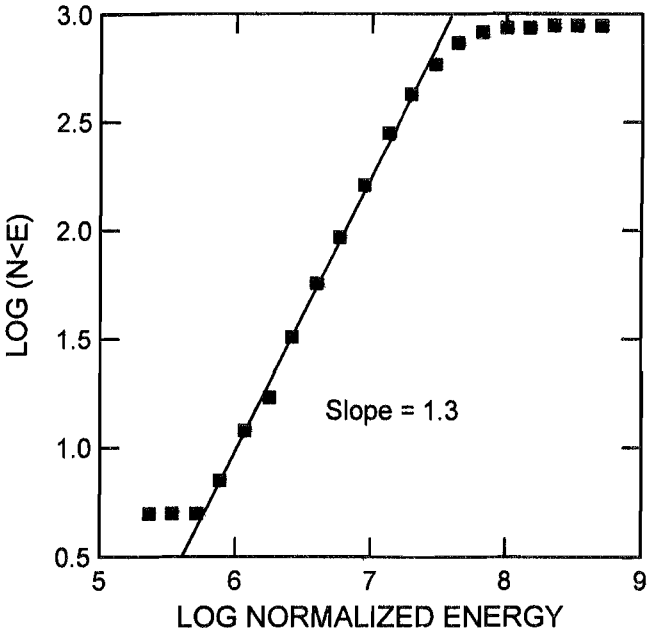

Determination of b-value from event energy distribution. "Normalized energy" (E) is calculated by summing individual channel energy counts premultiplied by square of distance between corresponding geophone and event location, and then dividing by number of such channels used to determine event location.

OTHER STATISTICAL MEASURES OF MINE SEISMICITY

Other statistical measures of the spatial, temporal, and size aspects of stope-scale seismicity are briefly described below, along with pertinent comments derived from our experiences in attempting to apply them to the understanding and prediction of rock bursts.

EVENT MEAN LOCATION

If mining activity (including blasting) is confined predominantly to one side of the stope for a few days and then shifts to the other side, the mean event location position may move. Similarly, long-term mean event position may move upward and sideways as the remaining pillar is excavated. We examined mean event locations on a daily basis for several timeframes at the same stope. For example, figure 19, covering the same 65 days of the activity shown in figure 11, shows the temporal changes in the east, north, and depth coordinates of the mean event location. At this time, the top of the stope was approximately 24.4 m (80 ft) below the 4600 level, and the center of the stope was at a (northing,easting) position of about (8330,11900). It is striking that the north and east coordinate changes are so well correlated for the first 33 days. This indicates that mean locations shifted southwestward or northeastward. Since the stope itself is aligned with the silver vein, striking about N. 45° E. here, the activity is probably centered in the residual pillar, shifting back and forth along the vein. Note also the shift in mean north coordinate after the two large bumps on days 35 and 36. Monitoring mean locations can give information about structure that is stimulated by mining activity, especially if previously inactive structural elements suddenly become active. Sudden mean location shifts that are uncorrelated, and that quickly return to previous mean

Figure 19

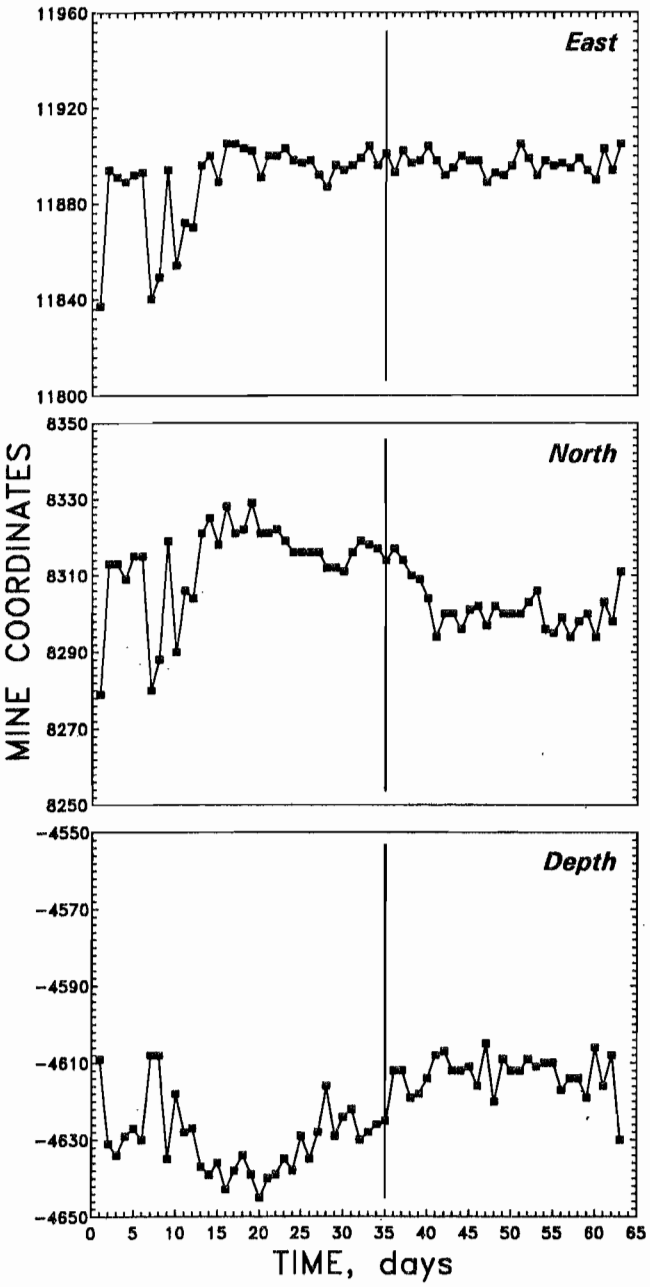

Daily mean event location coordinates (shown separately) for time period in figure 11. Vertical line at day 35 is just prior to the two rock bursts on August 4 and 5.

positions, may indicate a source outside of the local seismic net that has, in a sense, contaminated the local data. We are presently investigating the potential for using this method to discern interstope interactions.

INTER-EVENT DISTANCE DISTRIBUTION SKEWNESS

The inter-event distance distribution can be quantified by measures other than the two-point correlation dimension. The inter-event distribution skewness contains interesting and potentially useful information. The skewness is

$$Sk(X_n) = \frac{\sum [X_j - X_M)/\sigma]^3}{n}, \qquad (5)$$

where n is the total number of inter-event distances, X_M is the mean inter-event distance, σ is the distribution standard deviation, and the summation runs from $1 \le j \le n$. A perfectly symmetrical distribution has a skewness of zero. The greater the skewness, the longer the tail in the distribution. Also, the greater the skewness, the more clustered are the shorter inter-event distances. One needs to be careful here, since the volume in which the events occur may not be spherical. Elongated volumes will produce skewed inter-event distributions even for uniform, random data. Accordingly, the inter-event distribution skewness is normalized with respect to the skewness of a corresponding uniform, random set of synthetic locations of the same number and contained in the same volume as the real data. This *skewness ratio* has a magnitude proportional to the degree of nonrandom clustering in the data set. Skewness ratios as high as 10 have been measured immediately after a rock burst. The ratio typically decreases with time after a main shock, indicating increasing location dispersion. The part 2 report discusses attempts to use the skewness ratio as one of the sequence characteristics to distinguish postblast seismicity from postbump seismicity. The skewness ratio, or something like it (*38, 41-42*), could be used for time intervals instead of event pair distances, but we have not done so yet.

AFTERSHOCK RATE DECAY

After a main shock, the occurrence rate of nearby, subsequent events is known to decay following either an exponential or power law in time. That is, if $n'(t)$ is the event occurrence rate at a time t after the main shock, $n'(t)$ is proportional to either $\exp(-ct)$ or to t^{-p} where c or p are constants for some $t < T$. Exponential decay laws are typical of relaxation processes. Power law rate decay is often referred to as Omori's Law in earthquake seismology and has been shown to also apply to laboratory-scale seismicity (*43*). Sequences that have a power law rate decay are self-similar in time. Note that the time intervals between successive events are a small subset of

the set of all time intervals considered with the temporal correlation dimension. Typical values of p are close to 1 for earthquake sequences. The limiting time T for a large earthquake aftershock sequence characterized by a single exponent may be years. Aftershock sequences occur after both blasting and rock bursts or bumps in the mine. If uninterrupted by mining activity, the rate decay sequence can continue for several days. However, since production blasting may occur on a semiregular schedule, the practical limiting time T for mining-associated aftershock sequences in a single stope may be less than a day. Many of the production blasts induce one or more bumps or rock bursts shortly afterward (*7-8*), which should be distinguished from production blasts that do not. Contamination of a sequence by human activity in the stope or microseismic activity in other, nearby stopes, is also a problem often needing attention. For postblast and postbump sequences, we fitted

$$\log (n' [t]) = a + p \cdot \log (t) \qquad (6)$$

to obtain values of p for T = 2, 4, 8, and 16 h after the sequence initiation. Typical p values were found to vary between -0.2 and -0.8; they may be a function of T. Further results and discussion about this are presented in the part 2 report.

COEFFICIENT OF VARIATION

The ratio of the standard deviation to the mean of successive event time intervals was called the *coefficient of variation* by Kagan and Jackson (*25*). For a completely random, Poissonian occurrence sequence, this coefficient is equal to 1. If there is periodicity in the event occurrences, the coefficient is less than 1. If there is clustering in the successive event time intervals, the coefficient is greater than 1, and proportional to the degree of temporal clustering. Accordingly, this ratio is found to be much higher for time periods immediately following a blast or bump when the events occur closely together in time. For periods of relatively low activity, this ratio has a value closer to, but still greater than 1. So far, this measure has not proven useful for predictive purposes.

NEAREST NEIGHBOR AND NEXT EVENT STATISTICS

On the assumption that there is a zone of influence around each and every event, some correlation might be expected between nearest events and next events. In general, however, we have not found such a correlation. Figure 20 shows the distance versus time between nearest events for a typical aftershock sequence. During the sequence, next events may be located far from the previous event and, as time progresses, younger events may be located very close to older events. Therefore, there is no apparent correlation between the nearest event and the time it occurs with respect to its nearest neighbor. Obviously, event location uncertainty will be a big factor in ascertaining any such correlation. Figure 21 shows the

Figure 20

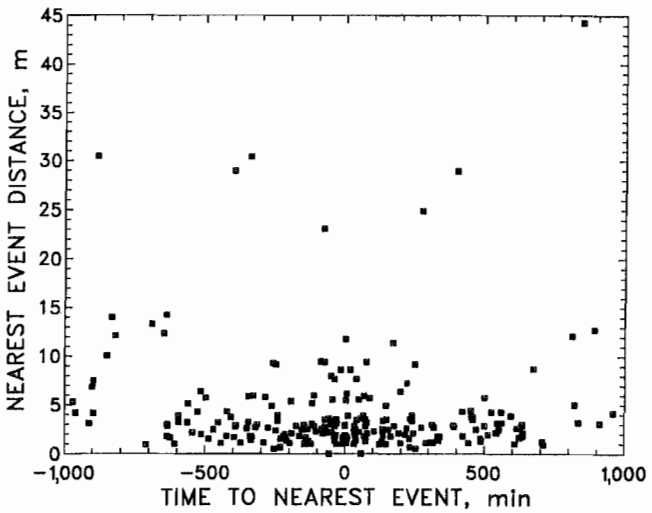

Distance to nearest event in sequence versus time when it occurs. Negative time means nearest event preceded the event. Although most events are within a few meters of their nearest event, they often occur a relatively long time before or after their neighbor.

Figure 21

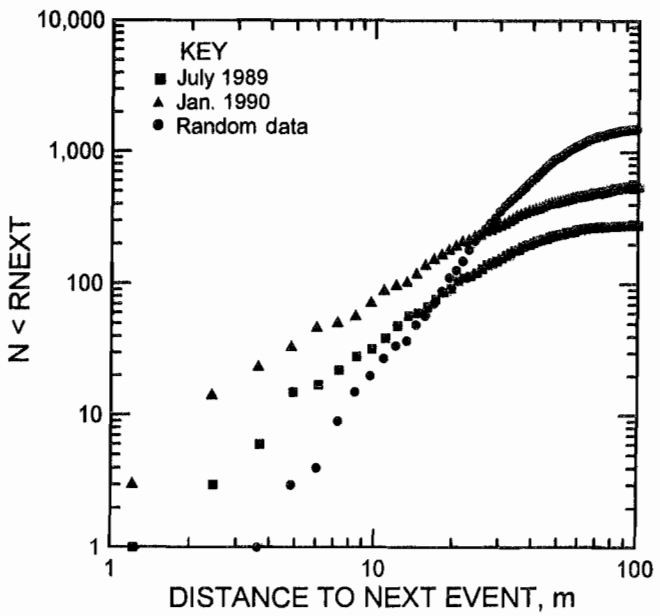

Distribution of distances to next located event. N<RNEXT is number of successive event pairs having a distance less than RNEXT, which is plotted on abscissa. About 1,000 random data for same stope are also shown.

distribution of the number of events having a distance to the next event less than a specific distance. This distribution, if linear in log-log space, would be similar to the correlation dimension calculated with equation 1. However, there we considered all inter-event distances and here we consider only the subset of next event distances. One problem with this and all measurements of *next* events is that the next event may not be the true next event in time, but instead the next located event in the catalog. However, the next event distributions for the sequences shown in the figure are clearly not random. Some evidence exists that there is an apparent artificial shadow zone around larger events that sometimes makes it impossible for the network to locate another event nearby very soon after the occurrence of the former event. This is probably because the waveform coda from the first event masks the primary arrivals from the true next, nearby event. It does not, therefore, get located and entered into the catalog. Rather, some event farther away becomes the apparent next event. For all these reasons, the nearest neighbor and next event statistics are not as useful as other measures described above.

EVENT LOCATION PLANARITY

The generic three-point method for finding planes in apparently unstructured or amorphous three-dimensional point patterns was developed by Fehler and coworkers (*44-45*), who applied it to earthquake location data. The underlying assumption, that earthquakes fall along one or more parallel planes, needs to be justified if the method is to be applied to small-scale microseismic and acoustic emission events detected in a mine. Any planarity found in a set of event locations by this method should be shown to be associated with a region-spanning structure. This structure might be natural (e.g., a joint set, a fault, or a mineral vein) or manmade (e.g., a stope or a drift). Failure to find any strong planarity in mining-associated microseismic event locations is also potentially useful information. The analysis should be done routinely if no visually obvious planarity is seen.

Briefly, the method has several sequential steps. First, since definition of any plane requires at least three points, all locations are taken three at a time in order to determine the strikes and dips of all possible planes in the data set. Minimum and maximum spacing between points so considered is optionally defined. The attitude of each plane defined by each three points can be identified by a normal vector or pole to the plane. These poles are grouped according to where they reside on an equal-area hemisphere projection. In practice, they are "binned," and the number of poles to planes falling into each equal-area bin, identified by its mean strike and dip, is tabulated. Nonrandom errors in event locations and other geometric considerations can introduce a bias in the distribution of binned poles. Therefore, the second step is to minimize potential bias by creating many different (we used 50) random artificial location data sets, each having the same number of events over the same volume as the original data set. Each such artificial data set is binned in the same manner as the original data set, and a statistical analysis of all the binned artificial data is made. The third step is to compare, bin by bin, the binned original real data with the binned artificial data set ensemble. The bin containing the most significantly different number of poles identifies the most likely orientation of a major plane in the original data. The more poles that bin contains, the better defined will be the attitude of the plane. Since each bin is of finite size, the orientation of the significant plane always has some uncertainty. The fourth step is to recover, from the original data set, those events that contributed to poles falling into the most significant bin. Subsequent steps in the analysis, as described by Fehler and others (*44-45*), may be taken to identify less significant planarity in the original location data.

Subsets of data encompassing large rock bursts or blasts were analyzed. The subsets did not, in general, contain equal numbers of locations. The relative strength of any planarity can, however, be evaluated by examining the percentage of coplanar events in a data set, or by comparing the number of standard deviations above the mean for the binned poles. As an example of the analysis, figure 22 shows the distribution of significant poles to planes found in data for the stope 307 data set shown in figure 23*A*. Table 1 summarizes results for stope 307 for two different subsets. The uncertainty in both strike and dip of the planes is typically ±5°. The "thickness" of the planar subset of points representing those events identified as part of the found planarity is typically 3 to 6 m. This is about the uncertainty in the horizontal component of individual event locations, but is also on the order of the stope width dimension.

Table 1.—Summary of major planes found in stope 307 rock-burst-associated seismicity

Data set	Total events	Coplanar events	Plane strike-dip
July 1989:			
All data plane 1	472	92	N. 80° E.-87° SE.
All data plane 2	472	161	N. 27° E.-89° SE.
Preburst	136	67	N. 73° E.-87° SE.
Postburst	336	139	N. 27° E.-89° SE.
January 1990:			
All data	563	172	N. 20° E.-86° SE.
Preburst	236	59	N. 21° E.-69° SE.
Postburst	327	113	N. 39° E.-87° SE.

Two significant planes were found when all events in the stope 307 July data set were examined, corresponding to the planes found when only preburst and postburst events were considered. Only one strong plane was found in the entire January data set (figure 22). After it was partitioned into preburst and postburst data sets, however, two slightly different planes emerged from the analysis. This illustrates how two closely oriented planes can modify results when all their events are combined. Figure 23*B* shows event location members for the plane found in the January 1990 data set shown in figure 23*A*. The orientation of the stope closely follows the orientation of the silver vein in this area. The vein is almost vertical and strikes between 25° and 45° east of north in this area. Mapped joints in this area are steeply dipping and typically strike northwest. Accordingly, it is concluded that the silver vein has a major effect on microseismic activity and apparently tends to closely concentrate events in its vicinity. Alternate conclusions involving the stress-concentrating power of the stope itself are also possible.

Figure 22

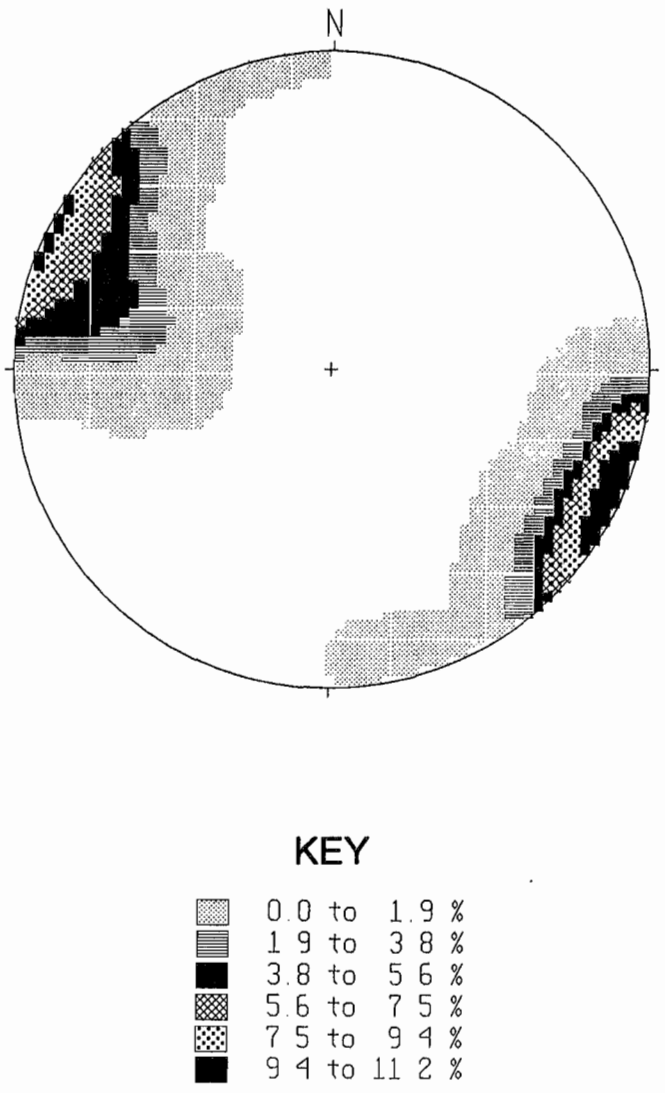

Normalized density of equal-area bins containing significant numbers of poles to potential planes in a data set. Plane containing most event locations strikes N. 20° E. and dips 86° SE.

Figure 23

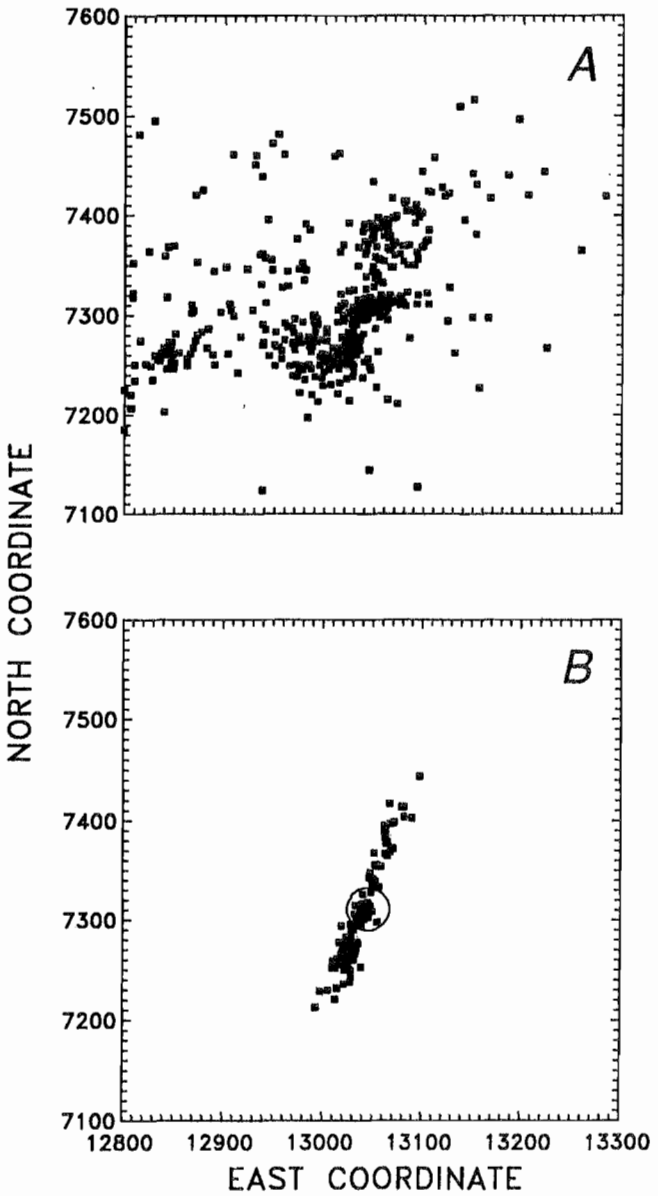

Event locations for a 3-day period and those events on a plane. A, Map of all 563 event locations, referenced to mine coordinates, for a 3-day period in January 1990. A rock burst, located at approximately 7310 North, 13050 East, occurred after event 236; B, 113 events on major plane found by plane-finding method discussed in text. Circle marks rock burst position.

DISCUSSION

In the unmined rock mass adjacent to stopes and drifts, it is likely that faults, joints, and other discontinuities exist on a variety of scales. That is, their lengths or areas, and their separations from each other have a distribution. It is tempting to try to associate the fractal point patterns with geologic structural scale invariance or even specific structural features (such as a fault or vein). As demonstrated above, typically a fraction of the events following a major shock are coplanar, the rest being distributed nearby. These coplanar events may be related to natural geologic features. Scale boundaries indicated by different fractal dimensions over different scale ranges may be related to similarly bounded structural scales. As also shown above, the scale range over which a single fractal measure is appropriate seems to depend on the size of the events included in the analysis. If the event sizes are fractal, and the event locations are fractal, we might expect similar fractality in the geology. There are some reports of fractal distributions for mapped joints and faults (*46-49*). Merceron and Velde (*49*) have even found differences in spatial fractality close to and far away from a mine. At this time we have not made similar analyses for the Galena Mine in the stope areas investigated seismically. However, we demonstrated elsewhere (*50*) that fracture systems that have a fractal distribution can be represented by fractal point patterns. Furthermore, seismic event location patterns that are spatially fractal strongly suggest that the parent fracture system is also fractal on scales at least as broad as the location point patterns. Thus, there is a good possibility of connecting the stope-scale seismicity to stope-scale rock mass fracture patterns and statistics.

The occurrence of mining-associated seismicity not immediately relatable to blasting episodes indicates that the volume of rock in which the entire mine is contained constitutes a system that is not in equilibrium. Regional tectonic stresses act continuously and are modified by the mine openings. At the stope scale, perturbations in the stress state caused by production or destress blasting are localized in space and time. The effects of these continuously superposed and changing stresses are nevertheless manifested in various fractal event location patterns. The Galena Mine is not currently being worked. Some seismicity continues to occur, however, so an opportunity exists for separating local perturbation effects from larger scale stress effects on longer time scales than studied here.

It is significant that in the time domain, during periods that encompass considerable mining activity, the distribution of event occurrence times is a homogeneous fractal for the scale of minutes to tens of days (figure 16). However, this long-time temporal fractality (scale-invariant clustering of event occurrences) is significantly weaker than the short-time fractality, which is highly influenced by the aftershock sequences during the period examined in figure 16. In this respect, aftershock sequences may be viewed as a sort of "contamination" of the stope's background seismicity. The high long-term temporal fractal dimension indicates the background seismicity may be a result of a superposition of random and other processes over the range of time scales considered. Kagan and Jackson (*25*) determined a similar fractal dimension of 0.8 to 0.9 for several long-term earthquake catalogs, thus also finding weak fractal clustering for larger scale seismicity.

The persistence of fractality over more than a month may be limited by the occurrence of relatively large events. Sprenke and others (*51*) found relative seismic quiescence for several months following large rock bursts at another mine in the Coeur d'Alene district, and we have noted short-term changes in temporal fractal dimension immediately after large rock bursts. However, in some cases, the same fractal dimension was obtained for comparable month-long time periods before and after large rock bursts or bumps (figures 16*A* and 16*B*). It would be interesting to examine the temporal correlation dimension for data from several stopes that include all events over a year or two, as was done by Smalley and others (*23*) for several years of earthquakes in the New Hebrides, to see if growing stope expansions significantly affect the long-term seismicity.

Swanson (*9*) has investigated kilometer-scale changes associated with larger events in this mine and has found support for the idea of interactions at that scale and linkage between large- and small-scale seismicity. On the larger scale, tectonic forces may be relatively more important than superimposed smaller stope-scale stresses, just as larger scale faults would be more important than smaller scale subsidiary fractures. We have not yet investigated the potential extension of scale invariance from the stope-scale seismicity discussed here to mine-wide scales in space and time. However, if it can be shown that fractality of the mining-related microseismicity persists over wider spatial and longer temporal scale ranges, a stronger case could be made for viewing the mine as a single system, reacting at all scales to cumulative mining.

Our data and analyses can be used to test various theories of rock mass failure and could lead to a better understanding of what occurs in the rock mass prior to and after large events. For example, relationships have been proposed between the various fractal dimensions in a fractured, seismically active system (*30, 32, 52*). What are the relationships, if any, between the correlation dimensions for time, space, and size attributes of mining-associated seismicity? Using the methods described above, we can compare correlation dimensions and b-values for the same data subsets to look for such relationships. There is an apparent relationship between the spatial correlation dimension and b-value for a mixed group of

aftershock sequences occurring in one stope over a year's time. Figure 24 shows an apparent *negative* correlation between the spatial fractal dimension and the b-value. Hirata (*31*) found a similar relationship from his examination of Japanese earthquakes. Hirata determined D = 2.3 - 0.73b, and we obtained D = 2.4 - 0.37b. This result is in contradiction to the positive correlation D = 2b hypothesized by Aki (*52*; see also *30*) for seismicity from ruptures on a single plane, but supports one of the models proposed by Main (*32*). For the same group of sequences, no apparent relationship was found between the temporal and spatial fractal dimensions, nor between the temporal fractal dimensions and the corresponding b-values. Further results and discussion about such relationships will be presented in the part 2 report.

Appropriately chosen random data sets are often the standard against which real data sets are compared. Significant deviations from randomness, or expected values, can be used as measures of the clustering properties of the real data sets (e.g., *17-19*). We used artificial random data in both the planarity-finding and skewness assessment methods, and the magnitude of the fractal dimension is itself a quantitative measure of the degree of clustering. Another very similar technique, "pair analysis statistics," has been used to study the spatial and temporal aspects of earthquake seismicity, and recently, mining-induced seismicity, by Eneva and colleagues (*38, 41-42*). Apparently, their method (and our skewness ratio method) can be used regardless of whether scale invariance is present, whereas

Figure 24

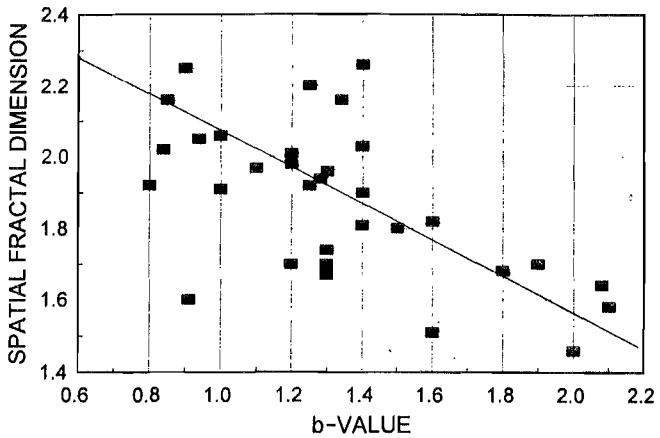

Cross-comparison of spatial fractal dimension and b-value for 32 aftershock sequences in 1989 to 1990 at stope 189: a negative correlation.

calculation of a correlation dimension does require (and therefore is a test of) self-similarity over a scale range. There are many possible physical processes that can give rise to nonrandom data, but the demonstration of fractality in seismicity is a strong indicator that the physical processes responsible for the seismicity also obey scale-invariant power laws (*53*).

CONCLUSIONS

In this first report, although we have concentrated on methodology, we also presented several important results. We demonstrated that stope-scale, mining-associated microseismicity has a fractal or scale-invariant nature. Furthermore, this nature is evident in the spatial, temporal, and size characteristics or attribute measures of the seismicity. As such, stope-scale microseismicity is similar to, and occupies a middle position between, larger scale earthquake seismicity and smaller scale rock acoustic emissions. The fractality is quantified by calculating a fractal dimension applicable over a bounded range of scales. In the cases considered here, fractality is apparent over ranges of approximately 1 to 100 m (3 to 328 ft), 10 s to a couple of months, and equivalent Richter magnitudes between about -5 and 0. Future studies may extend these ranges. The fractal dimensions calculated indicate that stope-scale seismicity is not random in space or time and is highly clustered immediately following blasts and rock bursts. Although this is not a new observation, the fractal dimension allows a quantitative measure of the degree of clustering and deviation from random patterns.

The usefulness of demonstrating fractality, for predictive or descriptive purposes, depends strongly on recognizing the various factors that can affect the calculation of fractal dimensions. Several methodological traps that can lead to a wrong calculation or conclusion were illustrated. These include not recognizing scale boundaries in the data, leading to inaccurate fractal dimensions, and making poor choices for time and space data windows, leading to false or unrecognized temporal changes. Additionally, we touched upon the effect of censoring data by size, (i.e., retaining and analyzing only larger events) whether purposefully or as a consequence of data acquisition limitations. In general, censoring diminishes the apparent scale range of fractality.

Finally, we described several other statistical methods to measure attributes of limited sequences of stope-scale microseismic events. The ensemble of all of these fractal and nonfractal attribute measures are used together in the part 2 report to characterize and group blast and rock burst aftershock sequences in this mine.

ACKNOWLEDGMENTS

The authors thank ASARCO, Inc., for their long-standing cooperation with the USBM in the field experiments at the Galena Mine, Wallace, ID. Data collection and field assistance by C. D. Sines, USBM engineering technician, over many years has resulted in the vast amount of raw data from that mine available for study. P. Swanson, USBM geophysicist, and C. Bufe, geophysicist of the U.S. Geological Survey, made several useful comments on an earlier version of this report.

REFERENCES

1. Blake, W., F. Leighton, and W. Duvall. Microseismic Techniques for Monitoring the Behavior of Rock Structures. USBM Bull. 665, 1974, 65 pp.

2. Coughlin, J. P. Software Techniques in Microseismic Data Acquisition. USBM RI 8691, 1982, 28 pp.

3. Repsher, R. C., and B. J. Steblay. Structural Stability Monitoring Using High-Frequency Microseismics. Paper in Proceedings of 26th U.S. Symposium on Rock Mechanics (Rapid City, SD), ed. by E. Ashworth. Balkema, 1985, pp. 707-713.

4. Steblay, B. J., B. T. Brady, and T. J. Swendseid. Innovative Microseismic Rockburst Monitoring System. Paper in Proceedings of 2nd International Symposium on Rockbursts and Seismicity in Mines (Minneapolis, MN), ed. by C. Fairhurst. Balkema, 1990, pp. 259-262.

5. McMahon, T. Rock Burst Research and the Coeur d'Alene District. USBM IC 9186, 1988, 45 pp.

6. Billington, S., F. M. Boler, P. L. Swanson, L. H. Estey. P Wave Polarity Patterns From Mining-Induced Microseismicity in a Hard Rock Mine. Paper in Proceedings of 31st U.S. Symposium on Rock Mechanics (Golden, CO), ed. by W. A. Hustrulid and G. A. Johnson. Balkema, 1990, pp. 931-938.

7. Swanson, P. L., and C. D. Sines. Characteristics of Mining-Induced Seismicity and Rock Bursting in a Deep Hard-Rock Mine. USBM RI 9393, 1991, 13 pp.

8. Riefenberg, J. Statistical Evaluation and Time Series Analysis of Microseismicity, Mining and Rock Bursts in a Hard-Rock Mine. USBM RI 9379, 1991, 15 pp.

9. Swanson, P. L. Mining-Induced Seismicity in Faulted Geologic Structures: An Analysis of Seismicity-Induced Slip Potential. Pure Appl. Geophys., v. 139, 1992, pp. 657-676.

10. Estey, L. H., P. L. Swanson, F. M. Boler, and S. Billington. Microseismic Source Locations: A Test of Faith. Paper in Proceedings of 31st U.S. Symposium on Rock Mechanics (Golden, CO), ed. by W. A. Hustrulid and G. A. Johnson. Balkema, 1990, pp. 939-946.

11. Coughlin, J. P., and R. L. Kranz. New Approaches to Studying Rock Burst-Associated Seismicity in Mines. Paper in Proceedings of 32nd U.S. Symposium on Rock Mechanics (Norman, OK), ed. by J. C. Roegiers. Balkema, 1991, pp. 491-500.

12. Swanson, P. L., L. H. Estey, F. M. Boler, and S. Billington. Accuracy and Precision of Microseismic Event Locations in Rock Burst Research Studies. USBM RI 9395, 1992, 40 pp.

13. ____. Mining-Induced Microseismic Event Location Errors: Accuracy and Precision of Two Location Systems. Pure Appl. Geophys., v. 139, 1992, pp. 375-404.

14. Boler, F. M., and P. L. Swanson. Observations of Heterogeneous Stope Convergence Behavior and Implications for Induced Seismicity. Pure Appl. Geophys., v. 139, 1992, pp. 639-656.

15. Feder, J. Fractals. Plenum, 1988, 283 pp.

16. Korvin, G. Fractal Models in the Earth Sciences. Elsevier, 1992, 396 pp.

17. Kagan, Y. Y., and L. Knopoff. Spatial Distribution of Earthquakes: The Two-Point Correlation Function. Geophys. J. R. Astron. Soc., v. 62, 1980, pp. 303-320.

18. Sadovskiy, M. A., T. V. Golubeva, V. F. Pisarenko, and M. G. Shnirman. Characteristic Dimensions of Rock and Hierarchical Properties of Seismicity. Izvestiya, Earth Phys., v. 20, 1984, pp. 87-96.

19. Ouchi, T., and T. Uekawa. Statistical Analysis of the Spatial Distribution of Earthquakes-Variation of the Spatial Distribution of Earthquakes Before and After Large Earthquakes. Phys. Earth Planet. Inter., v. 44, 1986, pp. 211-225.

20. De Rubeis, V., P. Dimitriu, E. Papadimitriou, and P. Tosi. Recurrent Patterns in the Spatial Behavior of Italian Seismicity Revealed by the Fractal Approach. Geophys. Res. Lett., v. 20, 1993, pp. 1911-1914.

21. Hirata, T., and M. Imoto. Multifractal Analysis of Spatial Distribution of Microearthquakes in the Kanto Region. Geophys. J. Int., v. 107, 1991, pp. 155-162.

22. Hirabayashi, T., K. Ito, and T. Toshii. Multifractal Analysis of Earthquakes. Pure Appl. Geophys., v. 138, 1992, pp. 591-610.

23. Smalley, R. F., J. L. Chatelain, D. L. Turcotte, and R. Prevot. A Fractal Approach to the Clustering of Earthquakes: Applications to the Seismicity of the New Hebrides. Bull. Seismol. Soc. Am., v. 77, 1987, pp. 1368-1381.

24. Papadopoulis, G. A., and V. Dedousis. Fractal Approach of the Temporal Earthquake Distribution in the Hellenic Arc-Trench System. Pure Appl. Geophys., v. 139, 1992, pp. 269-276.

25. Kagan, Y. Y., and D. D. Jackson. Long-Term Earthquake Clustering. Geophys. J. Int., v. 104, 1991, pp. 117-133.

26. Hirata, T., T. Satoh, and K. Ito. Fractal Structure of Spatial Distribution of Microfracturing in Rock. Geophys. J. R. Astron. Soc., v. 90, 1987, pp. 369-374.

27. Kusunose, K., X. Lei, O. Nishizawa, and T. Satoh. Effect of Grain Size on Fractal Structure of Acoustic Emission Hypocenter Distribution in Granitic Rock. Phys. Earth Planet. Inter., v. 67, 1991, pp. 194-199.

28. Kranz, R. L., T. Satoh, O. Nishizawa, K. Kusunose, M. Takahashi, K. Mausda, and A. Hirata. Laboratory Study of Fluid Pressure Diffusion in Rock Using Acoustic Emissions. J. Geophys. Res., v. 95, 1990, pp. 21593-21607.

29. King, G. The Accommodation of Large Strains in the Upper Lithosphere of the Earth and Other Solids by Self-Similar Fault Systems: The Geometrical Origin of b-Value. Pure Appl. Geophys., v. 121, 1983, pp. 761-815.

30. Huang, J., and D. L. Turcotte. Fractal Distributions of Stress and Strength and Variations of b-Value. Earth Planet. Sci. Lett., v. 91, 1988, pp. 223-230.

31. Hirata, T. A Correlation Between the b-Value and the Fractal Dimension of Earthquakes. J. Geophys. Res., v. 94, 1989, pp. 7507-7514.

32. Main, I. G. Damage Mechanics With Long-Range Interactions: Correlation Between the Seismic b-Value and the Fractal Two-Point Correlation Dimension. Geophys. J. Int., v. 111, 1992, pp. 531-541.

33. Brady, B. T., and F. W. Leighton. Seismicity Anomaly Prior to a Moderate Rock Burst: A Case Study. Int. J. Rock Mech. Min. Sci., v. 14, 1977, pp. 127-132.

34. Kneisley, R. O. Microseismic Data Analysis of Failure Occurrence in a Deep, Western U.S. Coal Mine: A Case Study. USBM RI 9228, 1989, 16 pp.

35. Smith, W. D. Evidence for Precursory Changes in the Frequency-Magnitude b-Value. Geophys. J. R. Astron. Soc., v. 86, 1986, pp. 815-838.

36. Zavyalov, A. D., and G. A. Sobolev. Analogy in Precursors of Dynamic Events at Different Scales. Tectonophysics, v. 152, 1988, pp. 277-282.

37. Xie, H., and W. G. Pariseau. Studies on Mechanism of Rock Bursts-Associated Seismicity Mines by Using Fractals and Damage Mechanics. Paper in Proceedings of 33rd U.S. Symposium on Rock Mechanics (Santa Fe, NM), ed. by J. Tillerson and W. Wawersik. Balkema, 1992, pp. 745-754.

38. Eneva, M., and R. P. Young. Evaluation of Spatial Patterns in the Distribution of Seismic Activity in Mines: A Case Study of Creighton Mine, Northern Ontario, Canada. Paper in Rockbursts and Seismicity in Mines (Proc.), ed. by R. P. Young. Balkema, 1993, pp. 175-180.

39. Volant, P., J-R Grasso, J-L Chatelain, and M. Frogneux. b-Value, Aseismic Deformation and Brittle Failure Within an Isolated Geological Object: Evidences From a Dome Structure Loaded by Fluid Extraction. Geophys. Res. Lett., v. 19, 1992, pp. 1149-1152.

40. Smith, L. A. Intrinsic Limits on Dimension Calculations. Phys. Lett. A, v. 133, 1988, pp. 283-288.

41. Eneva, M., and G. L. Pavlis. Application of Pair Analysis Statistics to Aftershocks of the 1984 Morgan Hill, California, Earthquake. J. Geophys. Res., v. 93, 1988, pp. 9113-9125.

42. Eneva, M., and M. W. Hamburger. Spatial and Temporal Patterns of Earthquake Distribution in Soviet Central Asia: Application of Pair Analysis Statistics. Bull. Seismol. Soc. Am., v. 79, 1989, pp. 1457-1476.

43. Hirata, T. Omori's Power Law Aftershock Sequences of Microfracturing in Rock Fracture Experiment. J. Geophys. Res., v. 92, 1987, pp. 6215-6221.

44. Fehler, M., L. House, and H. Kaieda. Determining Planes Along Which Microearthquakes Occur: Application to Earthquakes Accompanying Hydraulic Fracturing. J. Geophys. Res., v. 92, 1987, pp. 9407-9414.

45. Fehler, M., and P. Johnson. Determination of Fault Planes at Coalinga, California by Analysis of Patterns in Aftershock Locations. J. Geophys. Res., v. 94, 1989, pp. 7496-7506.

46. Barton, C. C., and E. Larsen. Fractal Geometry of Two-Dimensional Fracture Networks at Yucca Mountain, Southwest Nevada. Paper in Fundamentals of Rock Joints (Proc. Int. Symp.), ed. by O. Stephannson. Balkema, 1985, pp. 77-84.

47. Chiles, J. P. Fractal and Geostatistical Methods for Modeling of a Fracture Network. Math. Geol., v. 20, 1988, pp. 631-654.

48. Hirata, T. Fractal Dimension of Fault Systems in Japan: Fractal Structure in Rock Fracture Geometry at Various Scales. Pure Appl. Geophys., v. 131, 1989, pp. 157-170.

49. Merceron, T., and B. Velde. Application of Cantor's Method for Fractal Analysis of Fractures in the Toyoha Mine, Hokkaido, Japan. J. Geophys. Res., v. 96, 1991, pp. 16641-16650.

50. Kranz, R. L. Fractal Point Patterns and Fractal Fracture Traces. Paper in Proceedings of 1st North American Rock Mechanics Symposium (Austin, TX, June 1-3, 1994), ed. by P. P. Nelson and S.E. Laubach. Balkema, 1994, pp. 793-800.

51. Sprenke, K. F., M. C. Stickney, D. A. Dodge, and W. R. Hammond. Seismicity and Tectonic Stress in the Coeur d'Alene Mining District. Bull. Seismol. Soc. Am., v. 81, 1991, pp. 1145-1156.

52. Aki, K. A Probabilistic Synthesis of Precursory Phenomena in Earthquake Prediction, an International Review, ed. by D. W. Simpson and P. G. Richards. AGU, 1981, pp. 566-573.

53. Ito, K. Towards a New View of Earthquake Phenomena. Pure Appl. Geophys., v. 138, 1972, pp. 531-548.